Nonlinear Structural Performance and Seismic Fragility of Corroded Reinforced Concrete Structures: Modelling Guidelines

Ebrahim Afsar Dizaj[a*], Mohammad M Kashani[b]

[a]Assistant Professor, Department of Civil Engineering, Azarbaijan Shahid Madani University, Tabriz, Iran. (corresponding author), Email: ebrahim.afsardizaj@azaruniv.ac.ir

Address: Iran, Tabriz, Azarbaijan Shahid Madani University, Faculty of Engineering, Department of Civil Engineering
Phone number: +989141581825

ORCID: https://orcid.org/0000-0002-7755-9983

[b]Associate Professor, Faculty of Engineering and Physical Sciences, University of Southampton, Southampton, SO17 1BJ, United Kingdom, Email: mehdi.kashani@soton.ac.uk
ORCID: https://orcid.org/0000-0003-0008-0007

Nonlinear Structural Performance and Seismic Fragility of Corroded Reinforced Concrete Structures: Modelling Guidelines

Ebrahim Afsar Dizaj[a*], **Mohammad M Kashani**[b]

[a]Assistant Professor, Department of Civil Engineering, Azarbaijan Shahid Madani University, Tabriz, Iran. (corresponding author), Email: ebrahim.afsardizaj@azaruniv.ac.ir

[b]Associate Professor, Faculty of Engineering and Physical Sciences, University of Southampton, Southampton, SO17 1BJ, United Kingdom, Email: mehdi.kashani@soton.ac.uk

Abstract

The current paper provides modelling guidelines for nonlinear analysis and fragility assessment of corrosion damaged reinforced concrete (RC) structures. A systematic guideline is proposed to model the adverse impact of corrosion on mechanical properties of steel and concrete materials including the negative impact of corrosion on inelastic buckling and Low-Cycle Fatigue (LCF) degradation of reinforcing bars. The proposed fibre-based modelling technique is capable of simulating the spatial variability of localised corrosion and the influence of corrosion on Damage States (DS). Corrosion-dependent pushover and cyclic analyses, Incremental Dynamic Analyses (IDAs), and fragility analyses carried out on three different case studies: (*i*) a cantilever square RC column, (*ii*) a cantilever circular RC column and (*iii*) a RC frame. The analyses results indicate that corrosion significantly affects the DS, sequence of failure mode, flexural capacity, and energy dissipation capacity of RC structures. Moreover, alongside the corrosion, the geometry of RC components also affects their failure sequence, cyclic behaviour and energy dissipation capacity. It is shown that increasing degree of corrosion penetration results in the concentration of damage mainly in confined concrete.

Keywords: corrosion; IDA; fragility; fatigue; failure mode; energy dissipation

Nomenclature

$\varepsilon_{u,corr}$	fracture strain of corroded bars
$\sigma_{y,corr}$	yield strength of corroded bars
$\sigma_{u,corr}$	ultimate strength of corroded bars
$\varepsilon_{u,0}$	fracture strain of pristine bars
$\sigma_{y,0}$	yield strength of pristine bars
$\sigma_{u,corr}$	ultimate strength of pristine bars
ψ	mass loss percentage of longitudinal reinforcement
E_s	elastic modulus of steel
E_{sh}	post-yield modulus of steel
$\sigma_{yc,0}$	compressive yield stress of pristine bars
$\sigma_{yc,corr}$	compressive yield stress of corroded bars
β_c	regression coefficient
L	effective length of longitudinal reinforcing bars
D	diameter of longitudinal reinforcing bars
λ_p	slenderness ratio
D_{corr}	residual diameter of the corroded reinforcing bars
$2N_f$	number of half-cycles at fracture of steel material
α	material constant for pristine steel bars
Θ	material constant for pristine steel bars
a	regression coefficient
b	regression coefficient
c	regression coefficient
d	regression coefficient
α_{corr}	material constant for corroded steel bars
A_{ave}	average cross-sectional area of the corroded reinforcing bar
A_0	cross-sectional area of virgin reinforcement
β	pitting coefficient
μ_{pc}	mean of β

σ_{pc} standard deviation of β

$S_{y,0}$ yielding slip of pristine reinforcement

$S_{u,0}$ ultimate slip of pristine reinforcement

K_1 initial slope of the stress-slip curve

K_2 post-yield slope of the stress-slip curve

$S_{y,corr}$ yielding slip of corroded reinforcement

σ_c compressive strength of virgin concrete

λ reduction factor for compressive strength of concrete cover

κ a factor to consider bar diameter and surface

ε_{c0} strain at peak compressive strength of concrete

n number of bars in compression side of the section

ρ_{rust} ratio of volumetric expansion of corrosion products to original steel material

b_0 column section width

$\sigma_{c,corr}$ residual compressive strength of unconfined concrete cover

$\varepsilon_{cu,corr}$ compressive strain of confined concrete at the onset of fracture of corroded confinement

$\sigma_{cc,corr}$ peak compressive stress of confined concrete with corroded confinements

$\rho_{t,corr}$ volumetric ratio of corroded confinement

ψ_t mass loss percentage of confinement

$\rho_{t,0}$ volumetric ratio of pristine confinement

L_{eff} buckling length of vertical reinforcements

L_{col} column length

D_{col} column diameter or depth

ρ_l vertical reinforcement ratio

ρ_h horizontal reinforcement ratio

N_u axial compressive force on the column

A_g gross cross-sectional area of column

E cumulative work

R_j base shear of column at the j^{th} step of loading

Δ_j tip displacement of column at the j^{th} step of loading

ρ_l ratio of vertical reinforcement of column

ρ_h ratio of transverse reinforcement

ρ_{top} ratio of top longitudinal reinforcement of beam

ρ_{bot} ratio of bottom longitudinal reinforcement of beam

θ_{max} peak drift ratio of roof

μ_{ln} logarithmic mean of θ_{max}

σ_{ln} logarithmic standard deviation of θ_{max}

1. Introduction

Reinforced Concrete (RC) is a widely used construction material globally because of the availability of its constituent materials, the strength and economy it offers, and the flexibility of its forms (Anam and Shoma 2002). However, RC structures located in environmentally aggressive areas such as chloride-laden environments, are subjected to material deterioration over their service life. There is a considerable number of older major infrastructure worldwide that suffer from ageing and deterioration (Ghosh and Padgett 2010).

Several studies in the literature have focused on the effect of corrosion on the nonlinear behaviour of corroded structural components, long-term material performance, and proposing empirical relationships to predict the service life of RC bridges using accelerated corrosion procedures in the laboratory (Rodriguez et al. 1997; Cairns et al. 2005). More recently, several experimental studies have been conducted to investigate the effects of corrosion on the structural performance of RC members subject to cyclic loading (Ma et al. 2012; Meda et al. 2014; Guo et al. 2015a; Yao et al. 2019; Zhou et al. 2019; Ge et al., 2020). The state-of-the-art review paper by Kashani et al. (Kashani et al. 2019) indicates that there are significant gaps in either the numerical or experimental studies of deteriorated RC structures.

In recent years, the fibre element modelling technique (Spacone et al. 1996) has received a significant deal of academic attention for the nonlinear analysis of RC structures. Based on this technique, several models have been developed in the literature for nonlinear structural analysis and vulnerability assessment of corrosion damaged structures (Alipour et al. 2011; Guo et al. 2015b; Rao et al. 2016; Xu et al. 2020). These models are generally simplified models based on the reduced cross-sectional area of corroded reinforcement, and disregard other important consequences of corrosion, e.g. its adverse effect on inelastic buckling and LCF degradation of reinforcements. Alongside the fibre element modelling

technique, other modelling approaches such as multi-layered shell elements (Belletti et al. 2017; Belletti and Vecchi, 2018) and brick elements (Di Carlo et al. 2017) are also developed in the literature to simulate the nonlinear structural behaviour of the corroded components. Belletti et al. (2017) developed PARC_CL 2.0 crack model that can accurately simulate the behaviour of in-plane and out-of-plane shear critical RC members. This model updated later in (Belletti and Vecchi, 2018) as PARC_CL 2.1 to include the buckling of reinforcement in the constitutive material model of steel. Di Carlo et al. (2017) successfully verified their adopted solid brick elements modelling approach using the cyclic response of experimentally tested corroded and uncorroded column specimens.

However, disregarding the inelastic buckling of reinforcing bars and its adverse effect on low-cycle fatigue (LCF) of reinforcing bars, especially those damaged due to ingress of chloride ions into the concrete, might significantly overestimate energy dissipation capacity of deteriorated RC structures. Moreover, in the absence of clear guidelines, the previous studies adopted the DS of pristine structure for fragility assessment of deteriorated structures. However, the recent studies (Dizaj et al. 2018a, 2018b; Afsar Dizaj and Kashani (2020)) demonstrated that using the corrosion-independent DS might lead to unrealistic estimation of failure probability of deteriorated structures.

1.1. Research contribution and novelty

To address the above-mentioned shortcomings in the existing numerical models, the current research aims to provide a comprehensive modelling guideline for nonlinear structural analysis and fragility assessment of deteriorated RC structures. The important contributions of this study are (*i*) providing a step by step modelling guideline for nonlinear structural analysis of corrosion damaged RC structures with the emphasis on some of the previously neglected aspects (e.g. inelastic buckling and LCF degradation of rebars); and (*ii*) investigating the impact of proposed detailed modelling strategies on accurate prediction of structural performance and failure analysis of such structures. To this end, firstly based on the results of previous experimental studies and existing empirical equations, a systematic modification on existing constitutive uncorroded material models is provided. Subsequently, an

advanced fibre-based nonlinear finite element modelling technique for RC columns and RC frames is proposed. Then, using the proposed model, a series of nonlinear monotonic (pushover), cyclic and dynamic analyses are conducted on two hypothetical cantilever RC columns and a hypothetical RC frame with various degrees of corrosion. The corrosion-dependent cyclic analysis of RC columns shows the importance of simulating LCF in dissipated energy estimation of RC structures, especially those suffering from ageing and degradation. Moreover, results show that in RC columns increasing corrosion level results in the concentration of damage mainly in core confined concrete. For example, while in pristine circular column LCF precedes the Confined Concrete failure (CC failure), for slight to moderate corrosion, the failure sequence changes to CC failure followed by LCF. For severely corroded case, CC failure is the main governing failure mode.

It is important to clarify that the main focus of this study is on the flexural failure dominant RC structures, where even for severe corrosion condition the shear failure is not relevant.

2. A general view of the proposed modelling guideline

Fig. 1 provides a general view of the proposed modelling guideline and its implementation in nonlinear analyses. As Fig. 1 shows, the whole paper is divided into three main tasks, such as constitutive modelling, Finite Element (FE) modelling, and application in structural analyses. The constitutive modelling techniques are discussed in sections 3 and 4, and finite element modelling strategy is discussed in section 5. Finally, the application of the proposed modelling technique in structural analysis and seismic evaluation of deteriorating reinforced concrete structures are demonstrated in sections 6 and 7.

In the following sections, the above-mentioned tasks are illustrated in detail.

Task I: Constitutive Modelling (sections 3&4)

3. Reinforcing bars
Ductility, strength
Inelastic buckling,
Fatigue life,
Localised corrosion
Bar slippage

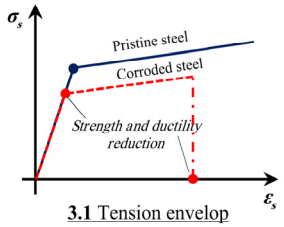

3.1 Tension envelop

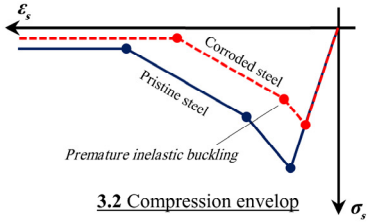

3.2 Compression envelop

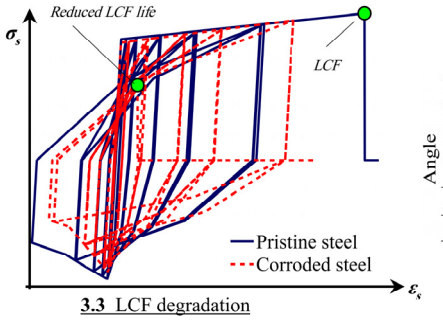

3.3 LCF degradation

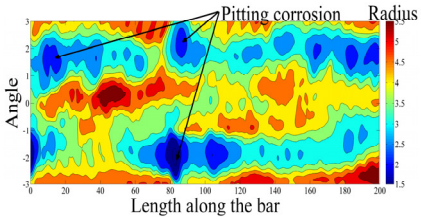

3.4 Variability of localised corrosion

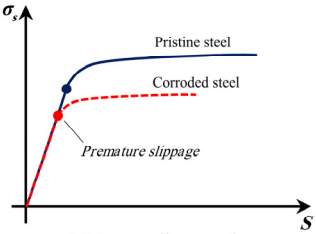

3.5 Stress-slip enevelp

4. Concrete
Premature spalling
Strength reduction
Premature crushing

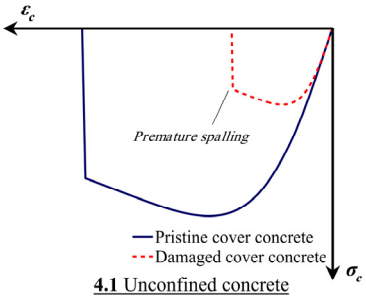

4.1 Unconfined concrete

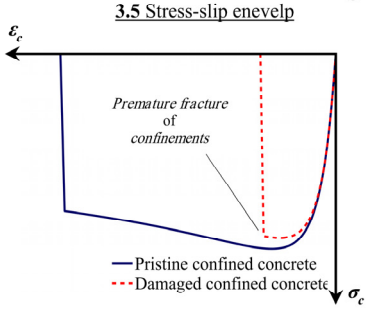

4.2 Confined concrete

Task II: FE Modelling (section 5)

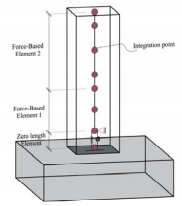

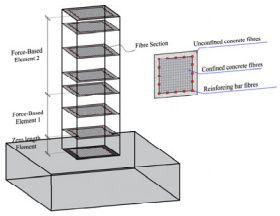

5.1 FE model of RC column

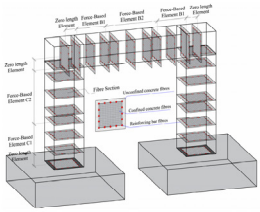

5.2 FE model of RC frame

Task III: Application in Structural Analyses (sections 6&7)

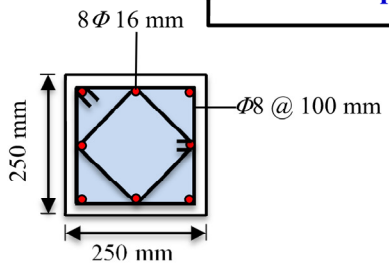

6.1 Square column

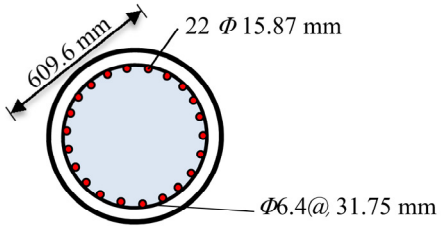

6.2 Circular column

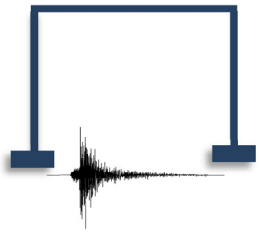

7. RC frame

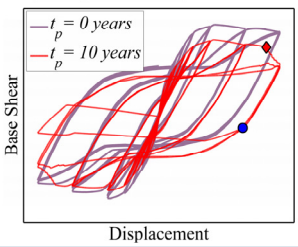

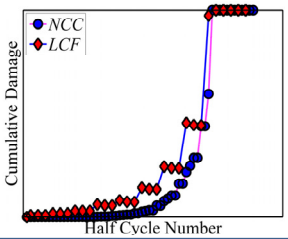

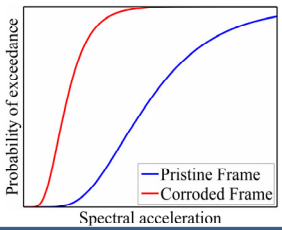

Fig. 1 A brief overview of the current study

3. Impact of corrosion on the mechanical behaviour of reinforcing bars

3.1. Monotonic tension

Several experimental studies have been dedicated to studying the negative influence of localised corrosion on monotonic tension envelope of reinforcing bars (Du et al. 2005a, 2005b; Apostolopoulos et al. 2006). Almost, all the above-mentioned studies confirm the adverse influence of corrosion damage on yield strength, ultimate strength, and ductility of reinforcing bars. Using accelerated corrosion procedure, Du et al. (2005a, 2005b) conducted comprehensive experimental studies on bare bars and embedded bars to explore the mechanical properties of corroded reinforcements. Based on the experimental results, Du et al. (2005a, 2005b) derived the following empirical linear relationship between residual strength and ductility of corroded reinforcements with their corresponding corrosion level (i.e. the percentage of mass loss) as Eqs. (1-3):

$$\frac{\varepsilon_{u,corr}}{\varepsilon_{u,0}} = 1 - 0.05\psi \tag{1}$$

$$\frac{\sigma_{y,corr}}{\sigma_{y,0}} = 1 - 0.005\psi \tag{2}$$

$$\frac{\sigma_{u,corr}}{\sigma_{u,0}} = 1 - 0.005\psi \tag{3}$$

where $\varepsilon_{u,corr}$, $\sigma_{y,corr}$ and $\sigma_{u,corr}$ are fracture strain, yield strength and ultimate strength of corroded bars, respectively; $\varepsilon_{u,0}$, $\sigma_{y,0}$ and $\sigma_{u,corr}$ are those of pristine bars, and ψ is mass loss percentage. Based on Du et al. (2005a) findings, corrosion does not affect elastic modulus and hardening strain of reinforcements. Eqs. (1-3) have been widely adopted to account for the impact of corrosion on mechanical properties of corroded bars under monotonic tension loading in numerical modelling (Alipour et al. 2011; Guo et al. 2015b; Rao et al. 2016). Using Eqs. (1-3), the nonlinear stress-strain relationship of corroded steel reinforcement in tension can be simulated using the bilinear model proposed by Balan et al. (1998):

$$\sigma_s = \frac{\sigma_{y,corr}}{2}\left[(1-\eta)+(1+\eta)\kappa-(1-\eta)\sqrt{\kappa^2+\mu}\right] \quad (4)$$

Where, η is the ratio of elastic modulus of steel (E_s) to post-yield modulus (E_{sh}); κ is the ratio of steel strain (ε_s) to its yielding strain ($\varepsilon_{y,corr}= \sigma_{y,corr}/ E_s$), and μ is a shape parameter. To define $\varepsilon_{u,corr}$, uniaxial *MainMax* material (available in OpenSees (McKenna 2011) library) is wrapped to the tension model mentioned in Eq. (1). Fig. 2 schematically compares the tension envelope of corroded reinforcing bars with that of pristine bars.

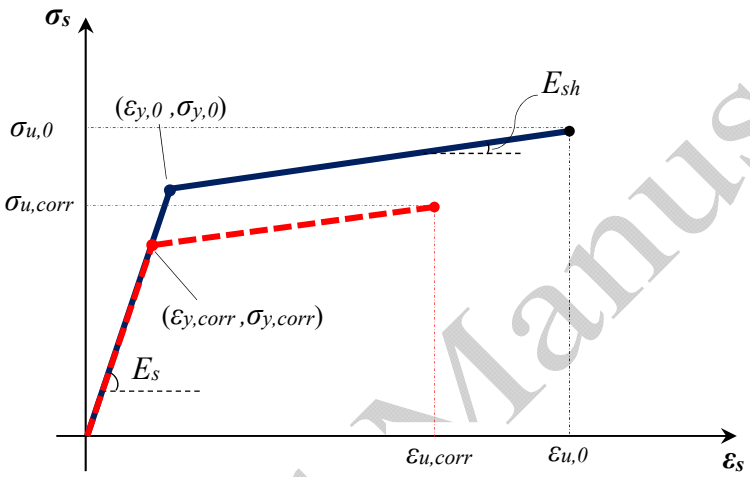

Fig. 2 Bilinear tensile stress-strain model of corroded and pristine reinforcing bars

3.2. Monotonic compression including inelastic buckling

Post buckling response of reinforcing bars is one of the important parameters, which affects the seismic performance, ductility, and energy dissipation capacity of RC structures in aggressive environments. Nevertheless, little studies in the literature have been dedicated to exploring the impact of corrosion on inelastic buckling behaviour of reinforcing bars. Kashani (2015a) conducted a set of experimental tests on reinforcing bars with various lengths, diameters and mass loss ratios under monotonic compressive loading, and proposed an empirical equation to modify the compressive yield strength as:

$$\frac{\sigma_{yc,corr}}{\sigma_{yc,0}} = 1-\beta_c\psi \quad (5)$$

where, $\sigma_{yc,0}$ and $\sigma_{yc,corr}$ are compressive yield stress of pristine and corroded bars, respectively. β_c, that is a regression coefficient to account for localised corrosion effects, is a function of L/D where L and D are effective length and diameter of longitudinal reinforcing bars, respectively. Further details are available in (Dhakal and Maekawa 2002; Kashani et al. 2015a). Fig. 3 shows the compression envelope of pristine and corroded reinforcement.

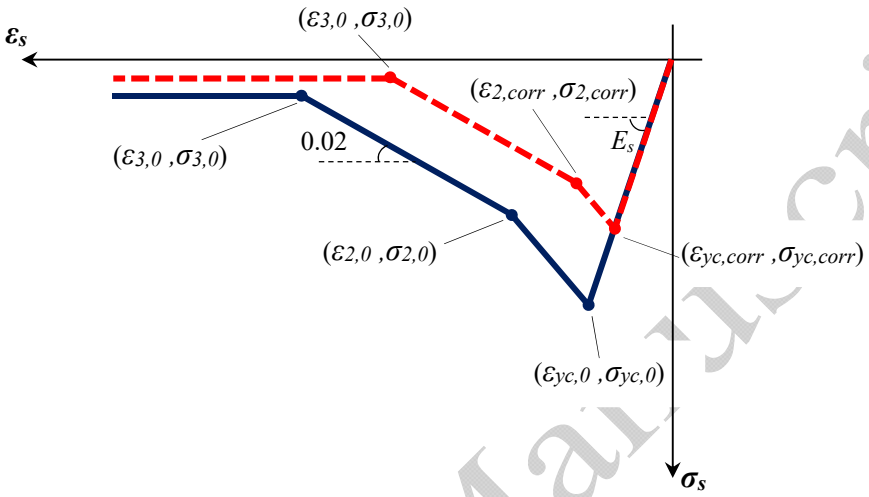

Fig 3. Compression envelop of pristine and corroded reinforcing bars

The required stress and strain points to define the compression backbone curve of pristine bars are obtained from Eqs. (6-9):

$$\varepsilon_{2,0} = \begin{cases} 7\varepsilon_{yc,0} & \varepsilon_{2,0} \le 7\varepsilon_{yc,0} \\ \varepsilon_{yc,0}\left[55 - 2.3\lambda_p\right] & \varepsilon_{2,0} > 7\varepsilon_{yc,0} \end{cases} \tag{6}$$

$$\sigma_{2,0} = \begin{cases} 0.2\sigma_{yc} & \sigma_{2,0} \le 0.2\sigma_{yc} \\ \phi\left[\sigma_{yc} + (\varepsilon_1 - \varepsilon_{yc})E_{sh}\right]\left[1.1 - 0.016\lambda_p\right] & \sigma_{2,0} > 0.2\sigma_{yc} \end{cases} \tag{7}$$

$$\sigma_{3,0} = 0.2\sigma_{yc} \tag{8}$$

$$\varepsilon_{3,0} = \frac{\sigma_{2,0} - \sigma_{3,0} + 0.02E_s\varepsilon_{2,0}}{0.02E_s} \tag{9}$$

where λ_p is slenderness ratio as:

$$\lambda_p = \sqrt{\frac{\sigma_{y,0}}{100}}\frac{L}{D} \tag{10}$$

and ϕ is proposed to be 1 for linear hardening. More details are available in (Dhakal and Maekawa 2002).

To define the backbone curve of corroded reinforcement, in Eqs. (6-10), $\sigma_{yc,0}$, $\varepsilon_{yc,0}$ and D are replaced by $\sigma_{yc,corr}$, $\varepsilon_{yc,corr}$ and D_{corr}, respectively; where D_{corr} is the residual diameter of the corroded reinforcing bar according to Eq. (11):

$$D_{corr} = D\sqrt{1-0.01\psi} \tag{11}$$

It should be noted that, for the small L/D, reinforcements might experience hardening behaviour at the post-yield branch. To show this, as an example, a typical compressive backbone curve for bars with L/D=4 is shown in Fig. 4.

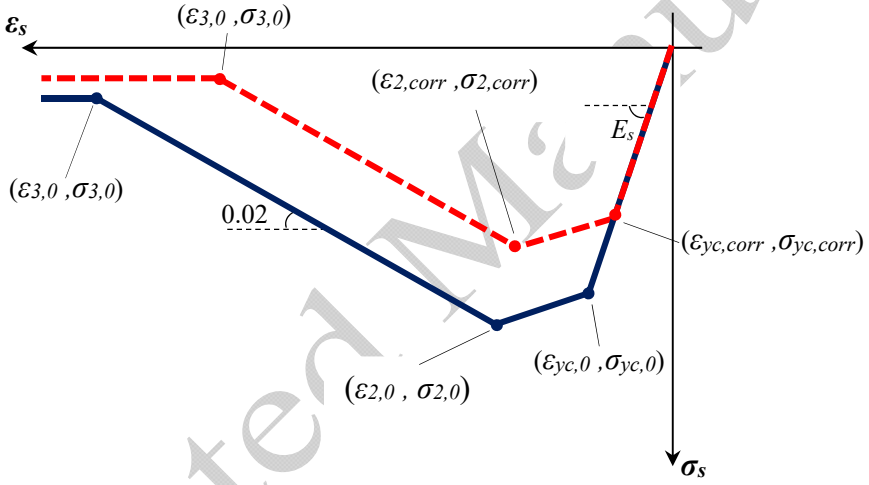

Fig 4. Example of compression envelop of reinforcing bars with L/D=4

3.3. Cyclic loading and LCF

LCF failure of reinforcing bars subject to cyclic loading is one of the critical damage states affecting the seismic performance and ductility of RC structures. In literature, several experimental and analytical studies have been carried out to investigate the influence of corrosion damage on LCF life of reinforcing bars (Apostolopoulos 2007; Fernandez et al. 2015; Kashani et al. 2013a).

The Coffin-Manson (Manson 1965) fatigue life model has been extensively adopted by researchers to estimate the fracture strain of reinforcing bars under repeated cyclic loading. In this model, the plastic strain amplitude (ε_p) is obtained as:

$$\varepsilon_p = \Theta_f (2N_f)^{-\alpha} \tag{12}$$

Where $2N_f$ is the number of half-cycles at fracture of steel material, and α and Θ are material constants. The experimental and computational study carried out by Kashani et al. (2015b), showed that fatigue life of reinforcements is greatly affected by its inelastic buckling behaviour; therefore, the combined effect of geometrical nonlinearities and LCF degradation might result in a significant reduction in energy dissipation capacity of RC components/structures. Kashani et al. (2015b) proposed Eqs. (13-14) to determine α and Θ:

$$\alpha = a\lambda_p - b \tag{13}$$

$$\Theta_f = c\exp(d\lambda_p) + e \tag{14}$$

Where a-e are regression coefficients presented in (Kashani et al., 2015b).

To account for the impact of corrosion on LCF failure of reinforcing bars, Kashani et al. (2015a), modified α as:

$$\alpha_{corr} = \alpha\left[1 + 0.004\psi\right] \tag{15}$$

Where α_{corr} is material constant for corroded steel bars. It was found that corrosion does not affect Θ.

3.4. Spatial variability of localised corrosion

The inelastic buckling of reinforcing bars, which is one of the main failure mechanism of RC structures, is considerably affected by the distribution pattern of pitted areas along the corroded bar length. This is because in pitted areas the load eccentricity, as well as minor and major axes, are changed (Kashani 2013b). Therefore, to investigate the seismic reliability of corroded structures, the distribution of pitted areas should be appropriately regarded in numerical modelling.

Spatial variability of pitting corrosion along the bar length has been extensively studied in previous studies (Stewart and Suo 2009; Darmawna 2010; Kashani et al. 2013b; Stewart 2009). The main goal of these analytical and experimental studies was to develop a time-dependent probability distribution functions to be used in seismic reliability assessments of RC structures.

Fig. 5 shows a contour plot of corrosion pattern in an example scanned corroded bar with 55.94 percentage of mass loss (Kashani et al. 2013b).

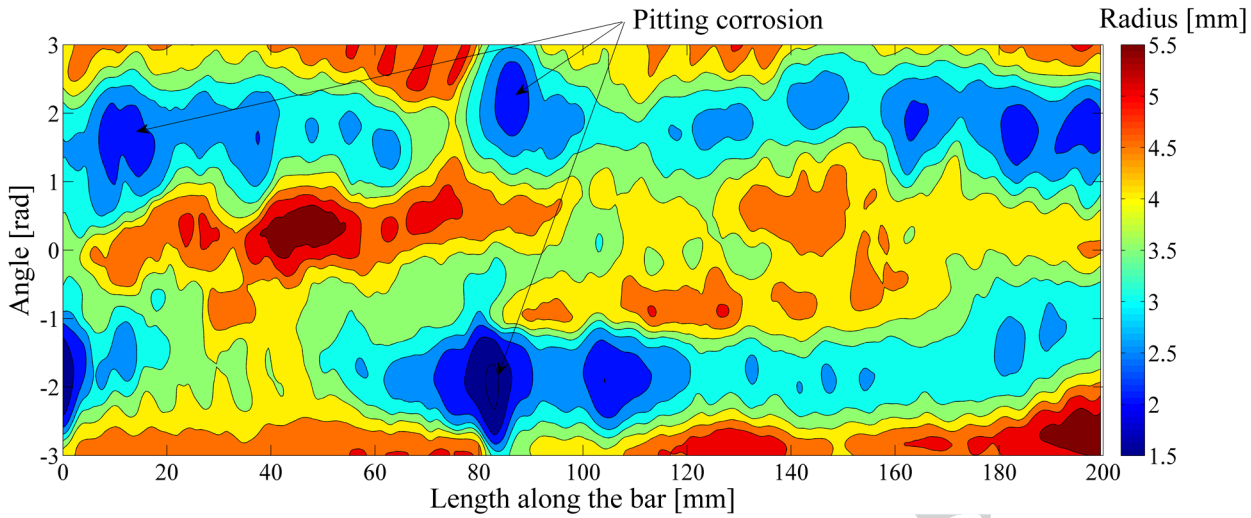

Fig. 5 Contour plot of corrosion pattern for a 55.94 % corroded bar

Using the data from optimal scanning procedure, Kashani et al. (2013b) proposed a time-variant stochastic lognormal distribution function to simulate the variability of pitted areas along the length of corroded reinforcement. Based on this model, the pitted area of the corroded reinforcing bar is obtained from Eq. (16):

$$A_{pit} = \beta A_{ave} \tag{16}$$

where A_{ave} is the average cross-sectional area of the corroded reinforcing bar which is obtained using Eq. (17):

$$A_{ave} = A_0\left(1-0.01\psi\right) \tag{17}$$

Where A_0 is the cross-sectional area of virgin reinforcement. In Eq. (16), β is pitting coefficient which is a random variable with the lognormal distribution. The mean (μ_{pc}) and standard deviation (σ_{pc}) of β are as Eq. (18) and Eq. (19), respectively:

$$\mu_{pc} = \exp\left(-0.00052\psi^{1.825} + \frac{(0.0006491\,\psi^{1.526})^2}{2}\right) \tag{18}$$

$$\sigma_{pc} = \left[\exp(-0.00104\psi^{1.825} + (0.0006491\,\psi^{1.526})^2)\right]\left[\exp((0.0006491\,\psi^{1.526})^2 - 1)\right] \tag{19}$$

3.5. Bond-slip behaviour

The well-designed RC members subject to reversal earthquake loading experience bond-slip rotation at their adjoining zone due to the strain penetration along the anchorage length of longitudinal reinforcement (Zhao and Sritharan 2007). Disregarding this phenomenon in the numerical simulations might cause an overestimation in lateral stiffness of RC structures; and therefore, results in an underestimation of their lateral displacement under seismic loading.

To account for the effects of bond-slip rotation at the end of RC members, the constitutive material model developed by Zhao and Sritharan (2007) can be used. This model is shown in Fig. 6(a).

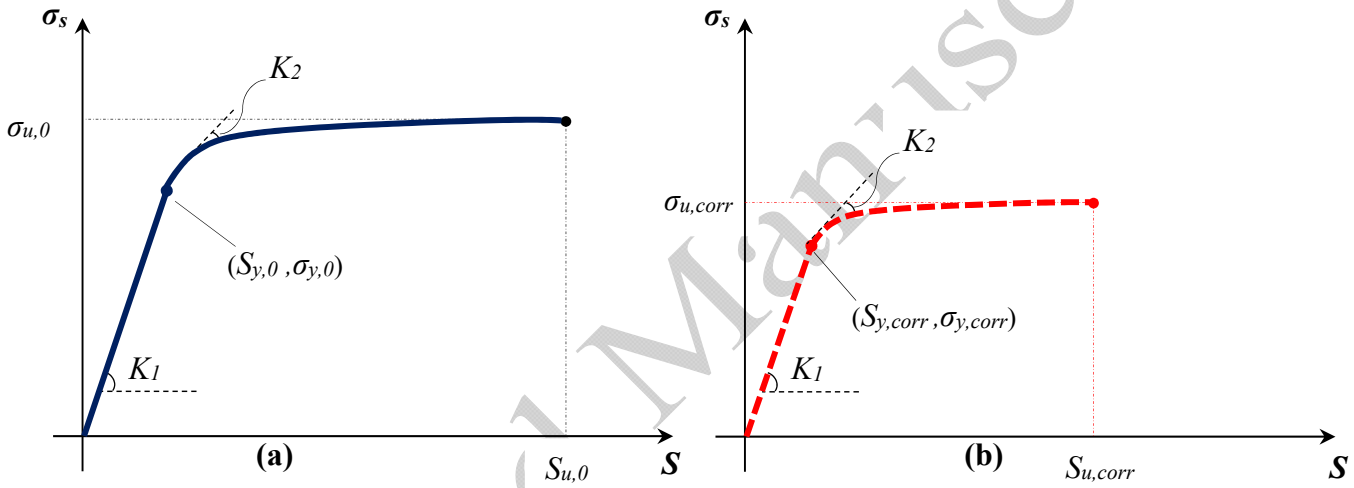

Fig. 6 Stress-slip material model: (a) pristine bars; (b) corroded bars

In Fig. 6 (a), $S_{y,0}$ is the yielding slip; $S_{u,0}$ is the ultimate slip, and K_1 and K_2 are the initial and post-yield slope of the stress-slip curve, respectively. More details are available in (Zhao and Sritharan 2007). Here, the original equation for the $S_{y,0}$ is simplistically modified based on Eq. (20) to account for the effect of corrosion:

$$S_{y,corr} = 0.0013\left[(1-0.01\psi)(1-0.005\psi)\frac{D\,\sigma_{y,0}}{\sqrt{\sigma_c}}\right]^{2.5} \quad (20)$$

Where σ_c is the compressive strength of virgin concrete. Fig. 6(b) shows the stress-slip model for corroded bars. To calculate $S_{y,0}$, in Eq.(20), it is enough to set ψ=0 (uncorroded case). Therefore, K_1 can be simply obtained as $\sigma_{y,0}/ S_{y,0}$ and $\sigma_{y,corr}/ S_{y,corr}$ for uncorroded and corroded reinforcement, respectively.

The suggested value of $S_{u,0}$ is 30~40$S_{y,0}$ (Zhao and Sritharan 2007). The value of K_2 can be simply obtained as the slope of the connecting line from yielding point to the ultimate point. To simulate the nonlinear stress-slip behaviour of the reinforcing bars, the uniaxial *Steel02* material model, available in the OpenSees, is used.

4. Impact of corrosion on the mechanical behaviour of concrete

4.1. Unconfined concrete

The consequences of corrosion are not limited to reinforcing bars only. Chloride induced corrosion of reinforcing bars produces expansive corrosion products surrounding the bar. Along the length of the bar, the greater volume of corroded steel leads to imposing split tensile stresses on the concrete cover; which eventually leads in premature longitudinal cover cracking and spalling (Vidal et al. 2004).

To consider the corrosion triggered cracking of cover concrete in numerical modelling, Coronelli and Gambarova (Coronelli and Gambarova 2004) proposed a reduction factor (λ) for compressive strength of concrete cover as:

$$\lambda = \frac{1}{1+\kappa\frac{\varepsilon_{ave}}{\varepsilon_{c0}}} \tag{21}$$

where, κ is a factor to consider bar diameter and surface which can be considered as 0.1; ε_{c0} is the strain at peak compressive strength of concrete, and ε_{ave} is the average tensile strain in cracked concrete which can be obtained from Eq. (22) (Coronelli and Gambarova 2004):

$$\varepsilon_{ave} = \frac{\pi n D\left[\rho_{rust}-1\right]\left[1-0.1\sqrt{100-\psi}\right]}{b_0} \tag{22}$$

Where n is the number of bars in compression side of the section; ρ_{rust} is the ratio of volumetric expansion of corrosion products to original steel material which can be taken as 2, and b_0 is the column section width. Therefore, the residual compressive strength of unconfined concrete cover ($\sigma_{c,corr}$) is obtained as:

$$\sigma_{c,corr} = \lambda\sigma_c \tag{23}$$

4.2. Confined concrete

The stress-strain response of confined concrete significantly depends on mechanical properties and volumetric ratio of transverse reinforcement (Priestley and Paulay 1992). In chloride laden environments, however, confining bars are corroded and ruptured before longitudinal bars as they are closer to the concrete surface. In such an environment, lack of sufficient confinement in RC columns results in deterioration of the compressive strength and ductility of the confined concrete core as well as premature buckling of longitudinal reinforcement.

A few studies have been conducted in the literature on corroded RC columns to investigate the negative effect of corrosion on the failure mechanism of confined concrete (Ma et al. 2012; Aquino and Hawkins 2007; Vu et al. 2017); and hence, there is not any solid constitutive material model in the literature to simulate the stress-strain response of deteriorated confined concrete. This is an open issue for future research. Nevertheless, an oversimplified procedure has been validated successfully by Dizaj et al. (2018a) against real experimental results. This procedure suggests that firstly the strain corresponding to the peak strength of sound transverse reinforcement ($\varepsilon_{ut,0}$) as well as its yield strength ($\sigma_{yt,0}$) should be modified by the same equations like Eq. (1) and Eq. (2), respectively, to get $\varepsilon_{ut,corr}$ and $\sigma_{yt,corr}$. Then, these two ($\varepsilon_{ut,corr}$ and $\sigma_{yt,corr}$) should replace those of pristine reinforcement in the empirical material models for confined concrete proposed by Mander et al. (1988) and/or by Kent-Scott-Park (Scott et al. 1982). Moreover, the ductility of the confined concrete model is decreased using Eq. (24) (Priestley and Paulay1992):

$$\varepsilon_{cu,corr} = 0.004 + 1.4\left[\frac{\rho_{t,corr}\sigma_{yt,corr}\varepsilon_{ut,corr}}{\sigma_{cc,corr}}\right] \tag{24}$$

where, $\varepsilon_{cu,corr}$ is the compressive strain of confined concrete at the onset of fracture of corroded confinement; $\sigma_{cc,corr}$ is peak compressive stress of confined concrete with corroded confinements, and $\rho_{t,corr}$ is the volumetric ratio of corroded confinement which is obtained from Eq. (25):

$$\frac{\rho_{t,corr}}{\rho_{t,0}} = 1 - 0.01\psi_t \tag{25}$$

where, ψ_t is mass loss percentage of confinement and $\rho_{t,0}$ is the volumetric ratio of pristine confinement.

It should be noted that currently, there is no stable fibre element formulation for axial-flexure-shear interaction. Some researchers (Jeon et al. 2015) have used springs to model shear failure, but it is uncoupled and does not account for axial-flexure-shear interaction. Moreover, there is currently no precise model in the literature for modelling shear failure of corroded beams and/or columns. Therefore, the focus of the current study is on flexural failure only, and in the considered RC structures the shear failure is not critical. Modelling shear failure of corrosion-damaged RC members is another important area for future research.

5. Finite element modelling of structures using nonlinear fibre beam-column elements

5.1. Proposed NFEMT for cantilever RC columns

Employing NFEMT, numerous models have been implemented in the literature to simulate structural behaviour of corroded structures/components (Alipour et al. 2011, Rao et al. 2016). These models, however, had some deficiencies such as disregarding the effect of corrosion on inelastic buckling and LCF of reinforcement as well as its adverse impact on DS. Kashani et al. (2016) developed an advanced NFEMT to simulate the nonlinear structural behaviour of corrosion damaged RC bridge piers. This unique numerical model can simulate the consequences of inelastic buckling and LCF degradation of corroded reinforcing bars on the global nonlinear response of RC columns. This model is later extended to incorporate the influence of corrosion on seismic damage thresholds, and verified by Dizaj et al. (2018a) against experimental test results. Further details are available in Dizaj et al. (2018a).

Force-Based fibre elements are widely used in the literature for nonlinear analysis of RC structures. Using one force-based element for a component, plasticity can be spread along the whole length of a member. However, Coleman and Spacone (2001) found that for the sections with softening response the simulation results using fibre-based elements might be biased due to strain localisation at the critical section of a member. The softening behaviour of RC sections is rooted in softening behaviour of concrete and post-buckling softening response of longitudinal reinforcement at the critical region of a member. To sort out the localisation problem due to the softening behaviour of concrete, Coleman and Spacone (2001) proposed a simple material regularisation method to adjust the ultimate compressive

strain of the concrete. The main assumption of this method was that the dissipated energy corresponding to the crushing of concrete (the area under the softening branch of the concrete material model) is constant. Further details on this model are available in (Coleman and Spacone 2001). This method is verified later by Pugh et al. (2012) in simulating nonlinear cyclic behaviour of RC shear walls. In RC columns, on the other hand, the post-buckling softening behaviour of vertical reinforcement significantly affects the strain localisation in the critical section of the column.

It is known that the post-buckling stress-strain response of reinforcement is averaged over a specific buckling length. Therefore, to solve the localisation problem due to the softening post-buckling response of vertical reinforcement, the integration length of the critical section of the column (first integration point) should be equal to the buckling length of the vertical reinforcement. However, it is impossible to adjust the integration length of the first integration point using one force-based element. Therefore, the proposed NFEMT suggest using two force-based elements.

Fig. 7 shows an overview of the proposed NFEMT for cantilever RC columns. As Fig. 7 shows, the whole length of the column is divided into a force-based element with 3 fibre-sections (Force-Based Element 1); a force-based element with 5 fibre sections (Force-Based Element 2), and a zero-length section element at the base of the column. The Force-Based Element 1 is considered to sort out the strain localisation problem at first fibre section due to the softening behaviour of compressive bars in the post-buckling region. To this aim, the length of this element is considered to be $6L_{eff}$ using 3 fibre-sections (integration points) with the Gauss–Lobatto integration scheme. This is because, using 3 integration point Gauss-Lobatto integration scheme, the weight of the first integration point will be 1/6, and therefore, the integration length of the first fibre section (critical section) will be equal to the buckling length of the vertical reinforcement (L_{eff}). The procedure of buckling length calculation is described by the detail in (Kashani et al. 2016).

For the second force-based element (Force-Based Element 2), based on the recommendation given by Lehman and Eberhard (2006) 5 integration points with Gauss-Lobatto integration scheme is used.

Moreover, the zero-length section element is used to address the slippage of reinforcing bars at the base of the column ((Zhao and Sritharan 2007)).

To validate the proposed NFEMT a set of 6 benchmark experimentally tested RC columns are selected. This set includes different cross-sectional shapes (circular, rectangular and square). Details of the selected column database are provided in Table 1. In this table, L_{col} is the column length; L_{col}/D_{col} is the ratio of the column length to diameter (or depth); ρ_l is vertical reinforcement ratio; ρ_h is horizontal reinforcement ratio and $N_u/A_g\sigma_c$ is the axial force ratio, where N_u is the axial compressive force on the column, A_g is the gross cross-sectional area of column.

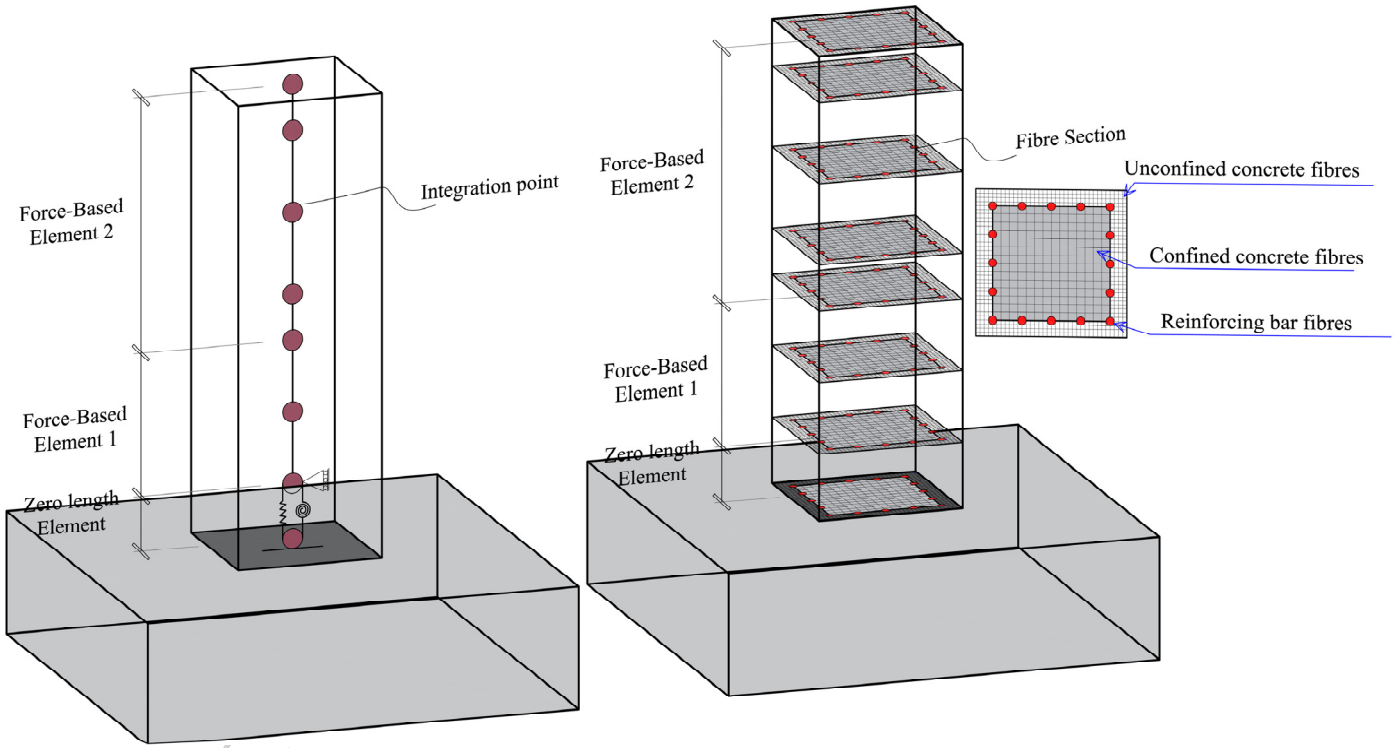

Fig 7. Overview of the proposed NFEMT for cantilever RC columns

Table 1. Details of experimental column data set

Column ID (Experiment Date)	Reference	Cross-sectional shape	L_{col} (mm)	L_{col}/D_{col}	ρ_l (%)	ρ_h (%)	$N_u/A_g\sigma_c$
415 (1998)	Lehman and Moehle (2000)	Circular	2438.4	4	1.49	0.7	0.07
1015 (1998)	Lehman and Moehle (2000)	Circular	6096	10	1.49	0.7	0.07
Henry 415p (1998)	Lehman and Moehle (2000)	Circular	2438.4	4	1.49	0.7	0.12
9 (1990)	Park and Paulay (1990)	Rectangular	2335	3	1.88	2	0.1
3 (1990)	Tanaka and Park (1990)	Square	1600	4	1.57	2.5	0.2
UC (2014)	Meda et al. (2014)	Square	1800	6	0.9	0.58	0.22

Fig. 8 shows the results of the proposed NFEMT against experimental results. As Fig.8 indicates, the proposed NFEMT successfully simulates the hysteretic response of experimental column specimens.

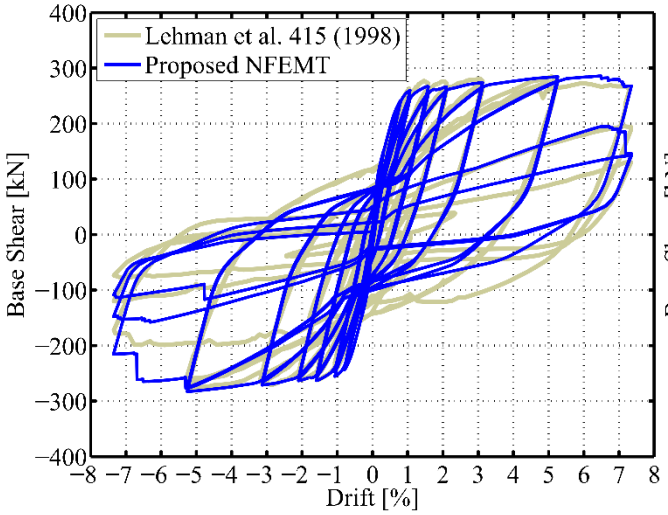
Lehman et al. 415 (1998)
Proposed NFEMT
Base Shear [kN]
Drift [%]

(a)

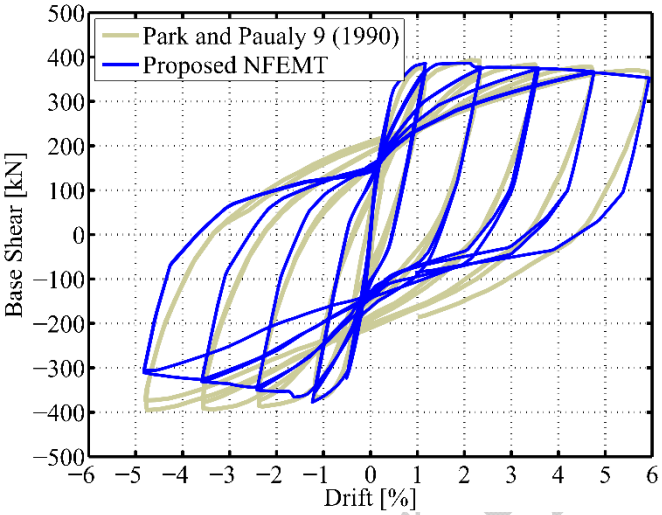
Park and Paualy 9 (1990)
Proposed NFEMT
Base Shear [kN]
Drift [%]

(b)

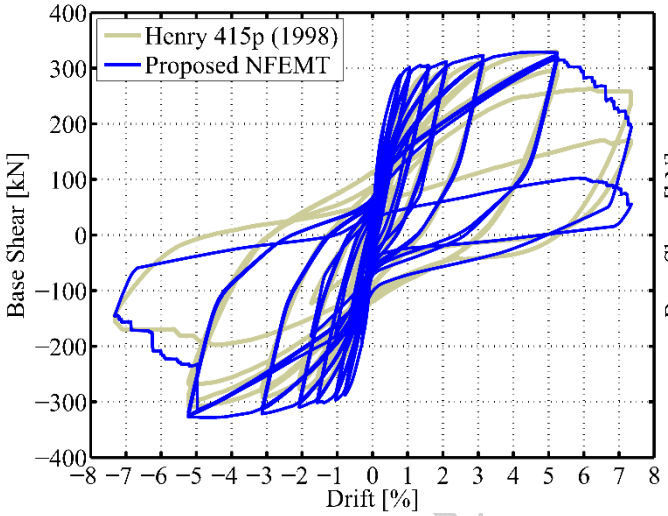
Henry 415p (1998)
Proposed NFEMT
Base Shear [kN]
Drift [%]

(c)

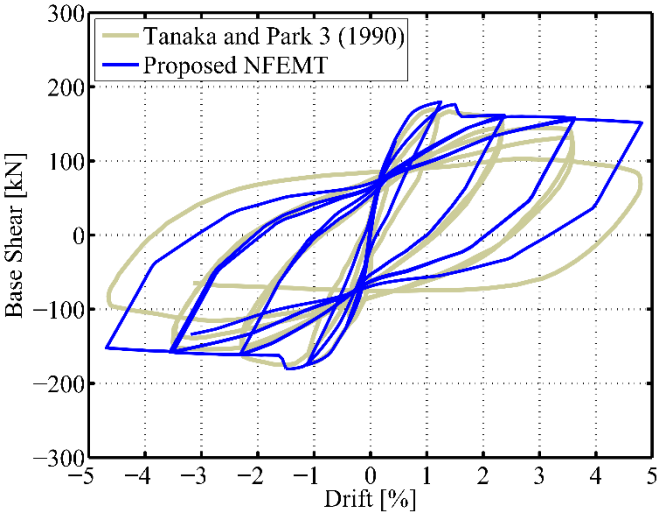
Tanaka and Park 3 (1990)
Proposed NFEMT
Base Shear [kN]
Drift [%]

(d)

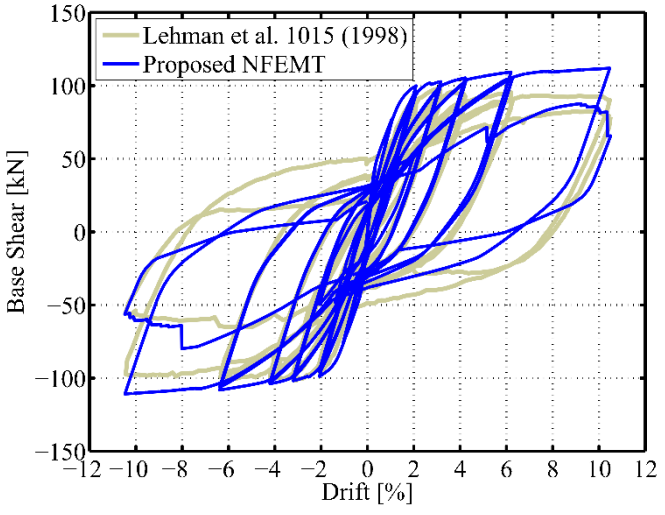
Lehman et al. 1015 (1998)
Proposed NFEMT
Base Shear [kN]
Drift [%]

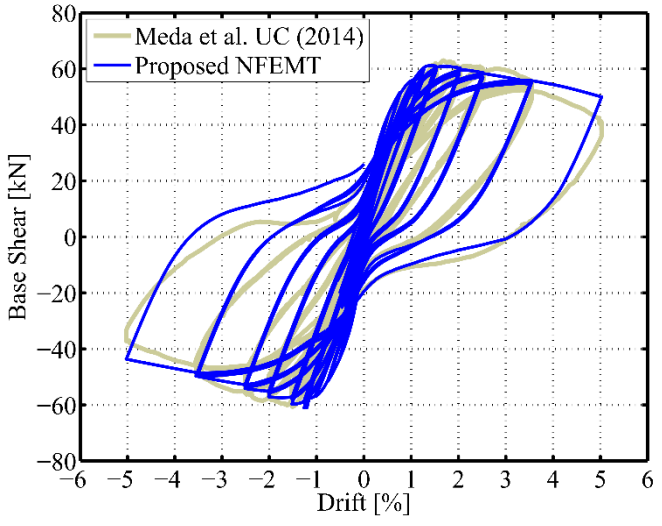
Meda et al. UC (2014)
Proposed NFEMT
Base Shear [kN]
Drift [%]

(e) (f)

Fig 8. Validating proposed NFEMT against experimental results: (a), (c) and (e) circular columns; (b), (d) and (f) rectangular columns

To investigate the accuracy of the proposed NFEMT the energy dissipation capacity of the simulated columns are quantified employing a trapezoid numerical integration scheme, as:

$$E = \frac{1}{2}\sum_{j=0}^{n-1}\left(R_{j+1}+R_j\right)\left(\Delta_{j+1}-\Delta_j\right) \tag{26}$$

Where E is the cumulative work (dissipated energy); R_j and Δ_j are base shear and column tip displacement at the j^{th} step of loading. The cumulative work of each considered column at each half cycle number is normalised to total cumulative work of corresponding experimental column to get the normalised cumulative work.

Fig. 9 shows that the calculated energy dissipation capacity of the simulated columns are in good agreement with those obtained from the experimental results. Therefore, the proposed NFEMT can accurately simulate the cyclic response of the experimental columns.

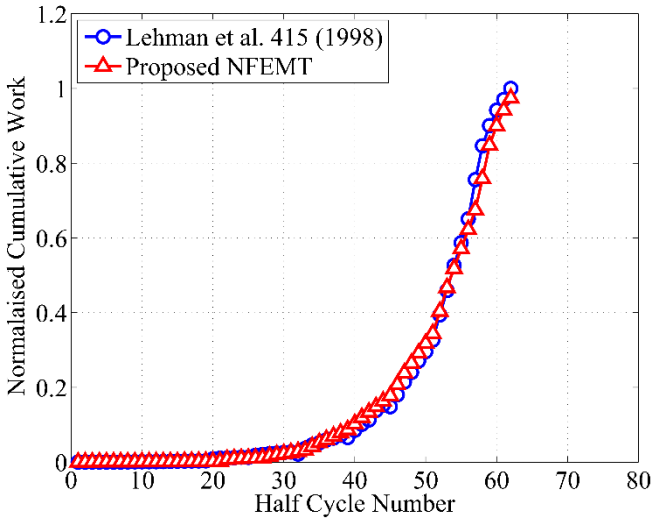

(a)

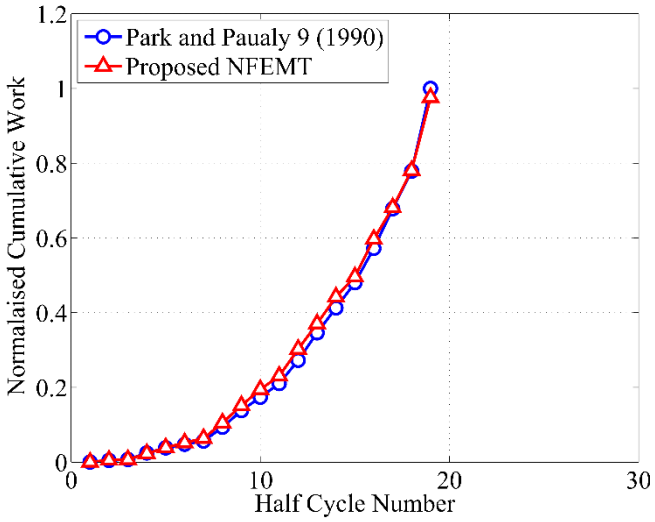

(b)

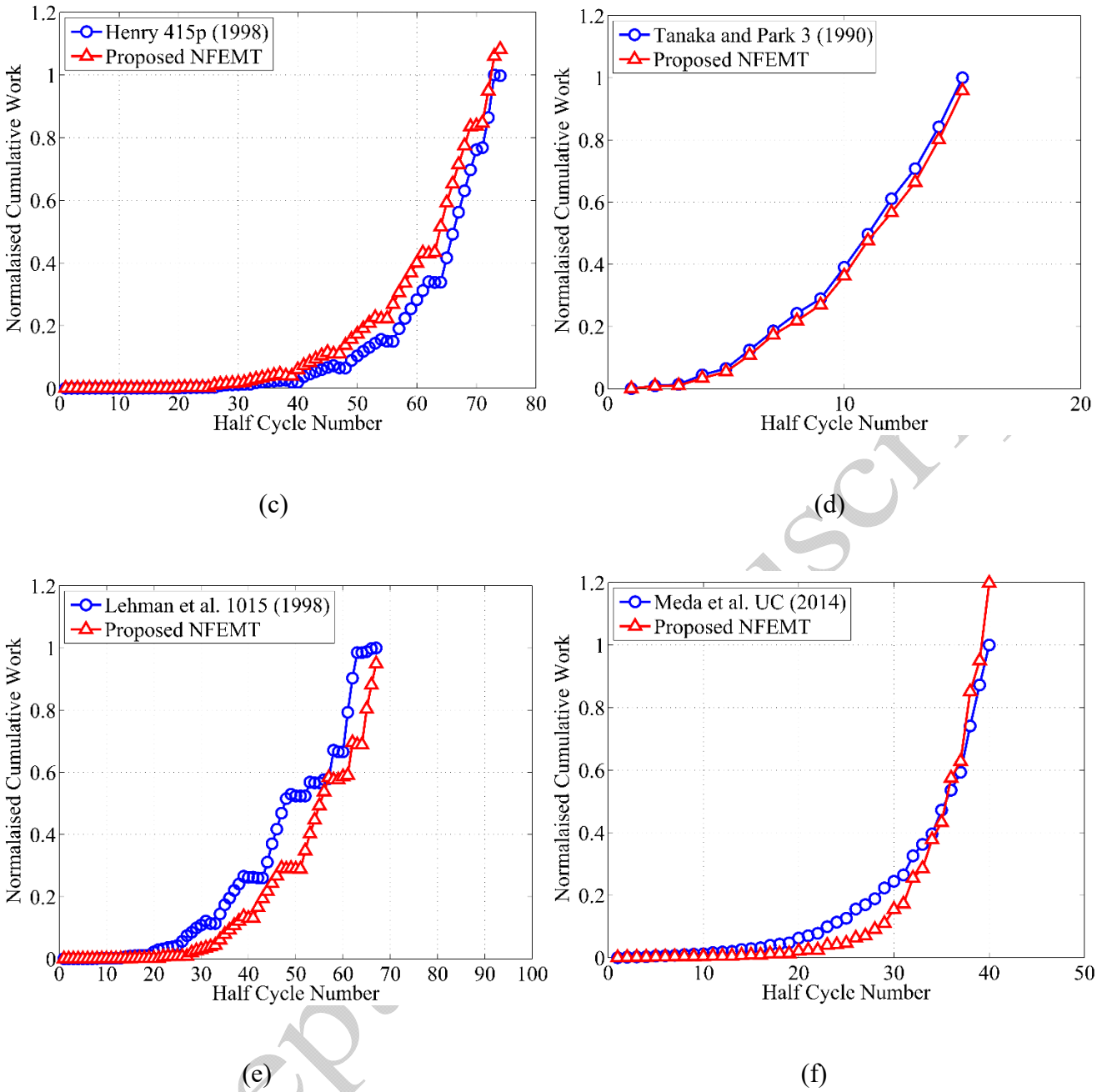

Fig 9. Comparing the results of the NFEMT with experimental results in term of energy dissipation capacity : (a), (c) and (e) circular columns; (b), (d) and (f) rectangular columns

To validate the capability of the proposed NFEMT in modelling the nonlinear cyclic response of corroded RC columns, the corroded column specimen tested by Meda et al. (2014) is adopted here as a reliable benchmark column. The details of this column (column CC) is similar to the column UC (given in Table 1). The average mass loss percentage of reinforcements is 20%. More details on the geometry and structural details of this column are available in (Meda et al. 2014). Fig. 10(a) shows that the

proposed NFEMT can successfully simulate the response of experimentally tested RC column. Moreover, Fig. 10(b) confirms this by comparing the cumulative energy dissipation of the experimental specimen with that of the proposed NFEMT at each half cycle.

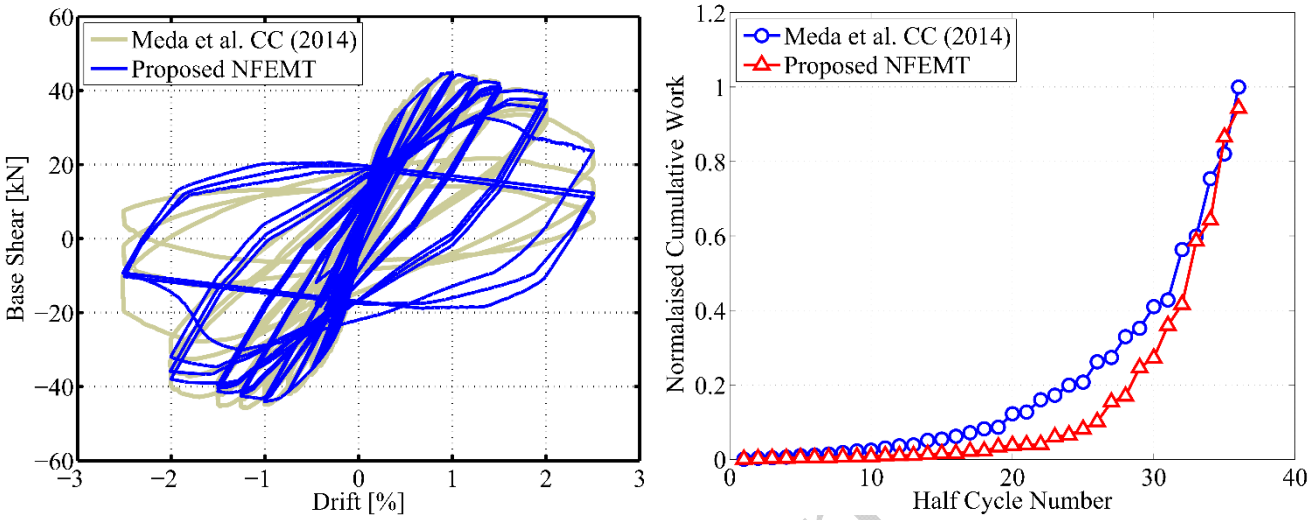

(a) (b)

Fig 10. Validating proposed NFEMT against experimental results of a corroded RC column: (a) hysteretic loops and (b) cumulative energy dissipation capacity

5.2. Proposed NFEMT for RC frames

The proposed NFEMT for cantilever RC column was extended in this section to establish the NFEMT for corrosion damaged RC frames, as shown in Fig. 11. To account for slippage of longitudinal bars at beam-column connection, four additional zero-length section elements at top of the column element and both ends of the beam element are defined. Further details are available in (Dizaj et al. 2018b).

The generic NFEMT of cantilever RC column and RC frame proposed in this section, are used in the next section as case studies to conduct nonlinear analyses.

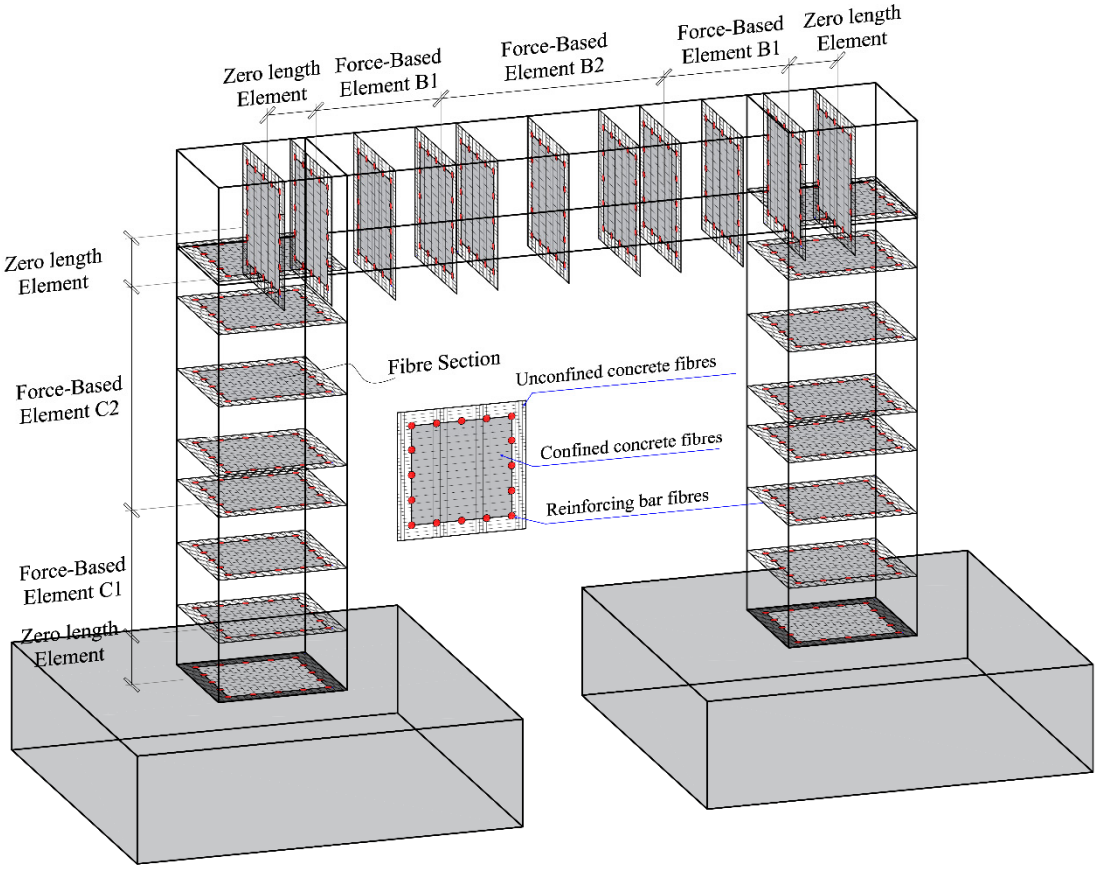

Fig 11. Fibre-based nonlinear finite element model for RC frame

6. Structural performance of corroded RC columns under static loading (monotonic and cyclic)

6.1. Proposed square RC column

In this section, an exemplar cantilever square RC column is adopted to demonstrate the capability of the proposed modelling guidelines in nonlinear time-dependent/corrosion-dependent analyses of corroded structures. The design of the selected square RC column is based on the Caltrans seismic design provisions (2010). The geometry and reinforcement details of the proposed hypothetical square column are shown in Fig. 12. The detailed assumptions of the properties of the square column are provided in Table 2. The calculated slenderness ratio (L_{eff}/D, where L_{eff} is the effective buckling length and D is the diameter of vertical reinforcing bars) of the compressive reinforcing bars is 10. L_{eff} is calculated based on the procedure proposed in (Dhakal and Maekawa 2002). The axial compression force ratio of the column is assumed as 0.1. The structural behaviour of the proposed column is simulated using the proposed NFEMT (Fig. 7). The stress-strain response of steel and concrete materials

are modelled using *Hysteretic* and *Concrete 02* material models (available in OpenSees) according to the procedure given in sections 2 and 3 of this paper, respectively.

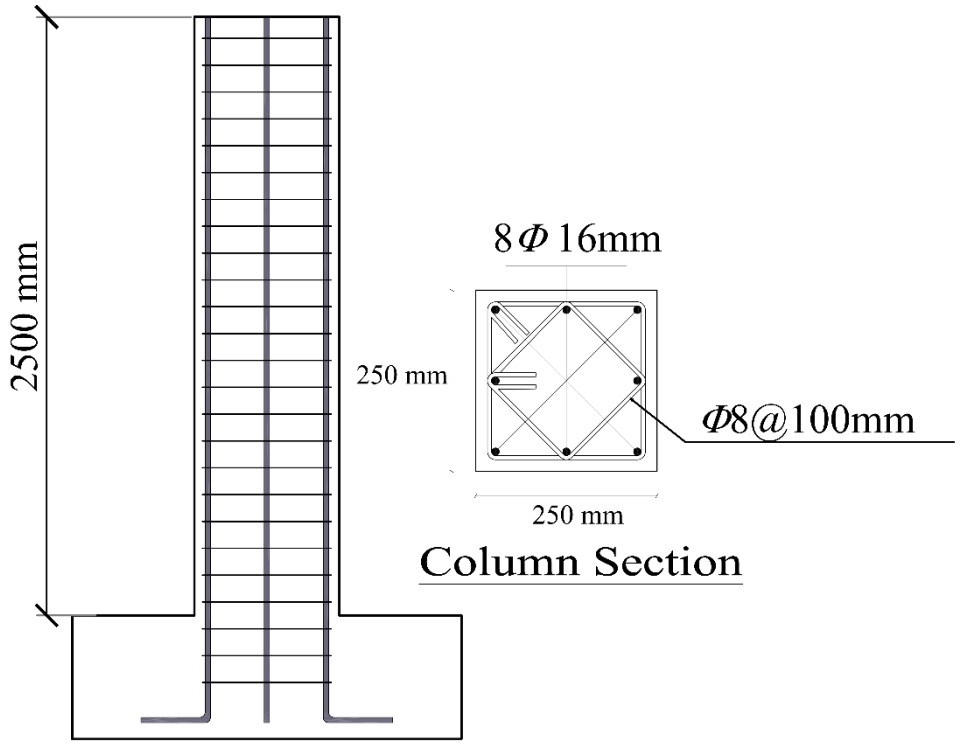

Fig 12. Geometry of hypothetical square RC column

To evaluate the structural performance of the hypothetical square column during different periods of its exposure to chloride ions, using the procedure provided in Dizaj et al. (2018a), the mass loss percentage of the transverse (ψ_t) and longitudinal bars (ψ) are calculated at 10, 30 and 80 years from corrosion initiation, and provided in Table 3. The considered times are representatively corresponding to slight corrosion; moderate corrosion and severe corrosion levels, respectively. It should be noted that the water to cement ratio is assumed to be 0.45.

Table 2. Material properties of the hypothetical square RC column

Material Properties	$\sigma_{y,0}$ [MPa]	$\sigma_{yt,0}$ [MPa]	$\sigma_{u,0}$ [MPa]	$\varepsilon_{u,0}$	E_s [MPa]	σ_c [MPa]
	530	530	630	0.18	210000	30

Table 3. Calculated percentages of mass loss

Time from corrosion initiation (t_p)	***0 years***	***10 years***	***30 years***	***80 years***
ψ (%)	0	5.4	11.5	22.4
ψ_t (%)	0	13.8	28.9	52.9

To conduct the nonlinear static (pushover and cyclic) analyses, it is assumed that the base of the column is fully fixed, but its top is allowed to move in the horizontal direction. The P-delta effect caused by the vertical load is also considered in the analyses.

Fig. 13 shows the result of monotonic pushover analyses of the square RC column for each considered time. In this figure, the horizontal displacement of the column tip is plotted against the normalised base shear; that is, the horizontal reaction of the base divided by its maximum value. For each case, DS including Longitudinal Reinforcement yielding (LR yielding), Longitudinal Reinforcement rupture (LR rupture) and CC failure (crushing) are mapped on the curves. As Fig. 13 shows, both the strength and ductility of the corroded columns are greatly declined in comparison with those of pristine column. Fig. 13 also shows that, as corrosion degree increases, the core CC failure takes place in relatively fewer displacements. This is due to the significantly reduced diameter of corroded transverse reinforcing bars that results in insufficient confinement of core concrete.

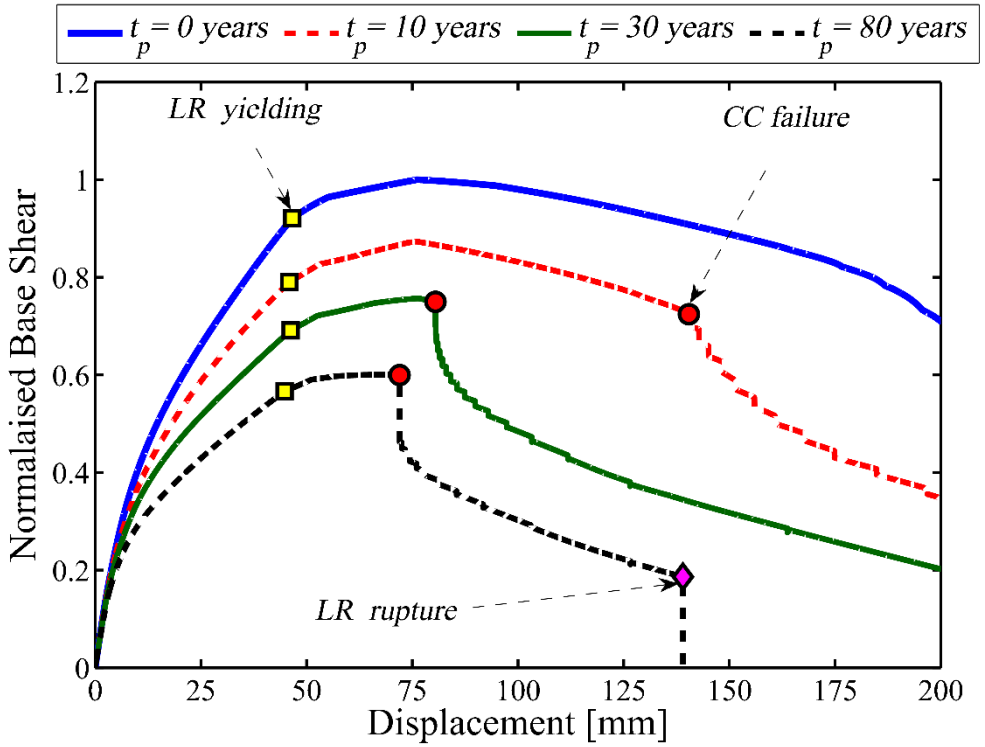

Fig 13. Results of corrosion-dependent pushover analysis

Moreover, while up to t_p=30 years, the failure of the column is caused by CC failure; for severely corroded column (t_p=80 years), the failure is governed by the sequence of CC failure and LR rupture. This is due to the significant reduction in the diameter of severely corroded reinforcement.

Fig. 14, compares the pushover results of the square RC column with and without considering the bond-slip effects (section 3.5) in numerical modelling. As can be seen in Fig. 14, neglecting bond-slip behaviour of the reinforcement at the base of the column results in an overestimation of lateral stiffness and underestimation of tip displacement of the column. In the other words, the results of pushover analysis are shifted to the left side when the bond-slip effects are disregarded. Therefore, to realistically simulate the nonlinear behaviour of the structure, modelling the bond-slip behaviour of the reinforcing bars at the adjacent of the column connection is necessary.

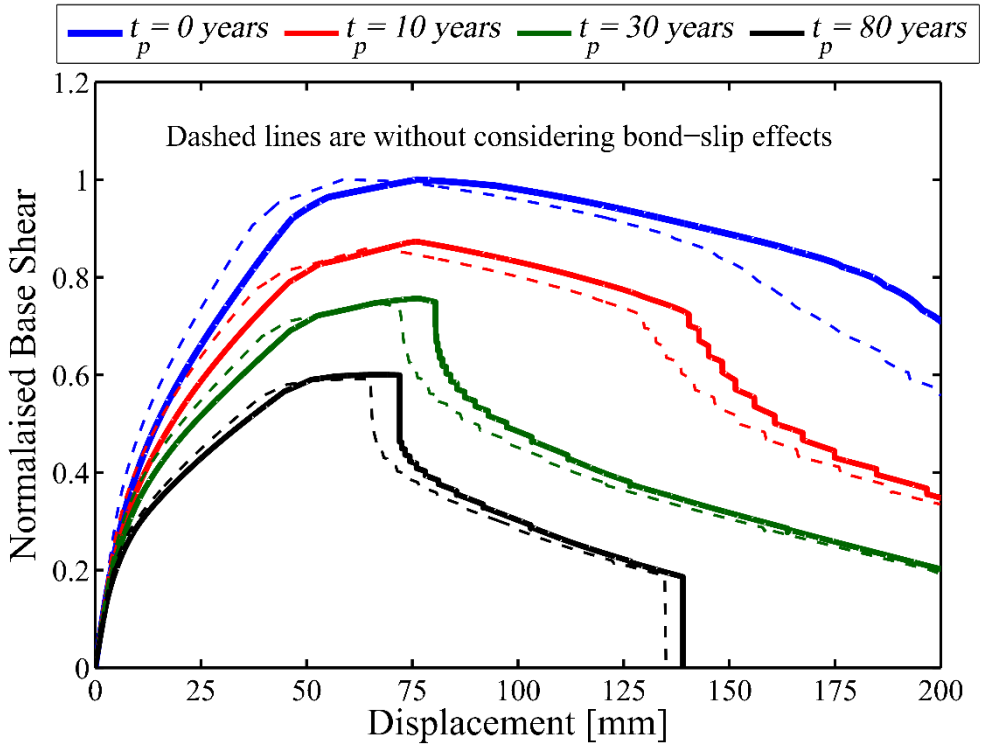

Fig 14. Comparing pushover results with and without considering bond-slip effects

However, the nature of repeated loading reversals and the structural responses under cyclic loadings might be different (mainly due to possible LCF degradation) with that observed in monotonic analyses. On this basis, to investigate the cyclic response of the considered square RC column as well as its energy dissipation capacity and failure sequences, a static cyclic analysis is conducted on each column using the loading protocol that is shown in Fig. 15. To capture the LCF degradation of longitudinal bars, the *Fatigue* material available in OpenSees is used along with the material model of reinforcing bars (section 3 of this paper). The values of α and Θ are considered to be -0.602 and 0.192 based on the Eqs. (13-14).

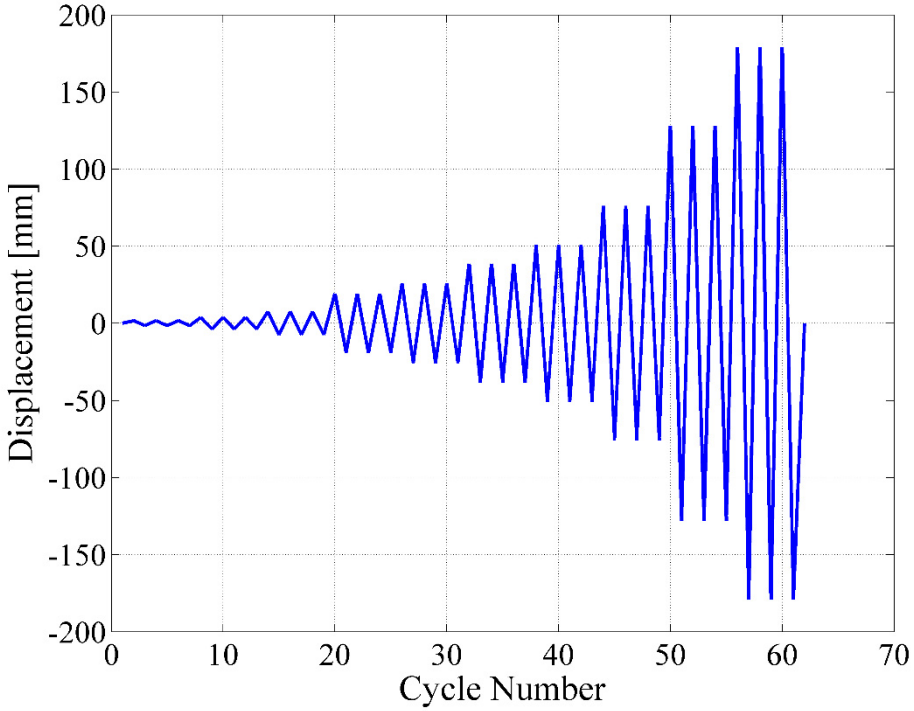

Fig 15. Proposed cyclic loading protocol

The hysteretic response of the square columns is shown in Fig 16. Fig. 16 shows that while in the pristine column, the reinforcing bars do not experience the LCF failure; all the considered corrosion damaged columns experience the LCF failure of reinforcement. For example, as can be seen in Fig. 16(c), the severely corroded column is collapsed after a few cycles due to the sequence of CC failure and LCF failure. This confirms that corrosion exacerbates the LCF degradation of reinforcing bars.

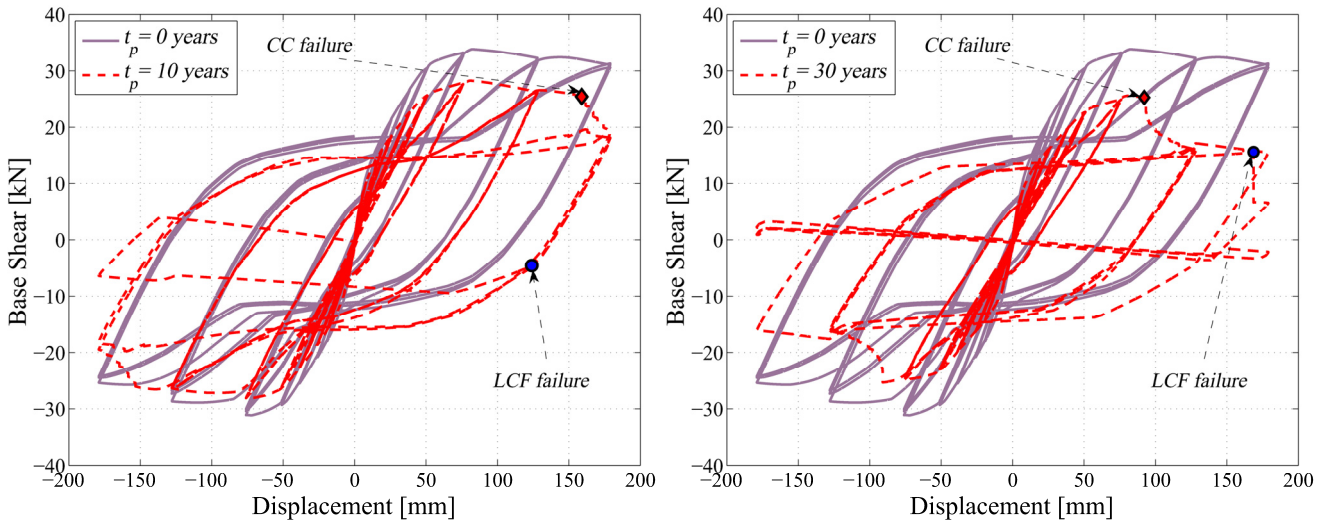

(a) **(b)**

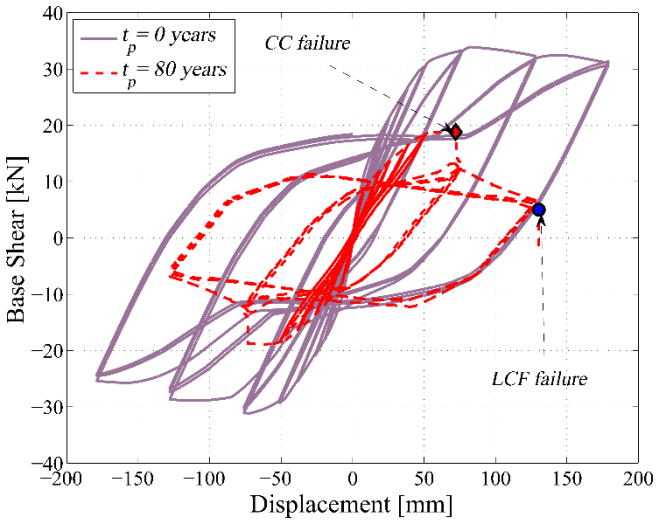

(c)

Fig 16. Comparing hysteretic loops of the pristine square column with that of: (a) column at t_p=10 years; (b) column at t_p= 30 years, and (c) column at t_p =80 years

To have a deeper sight on the trend of damage accumulation and failure sequence along with the increased number of cycles, in Fig. 17 the cumulative damage in confined concrete and LCF index are plotted at each half cycle number. To plot Fig. 17, for each column, the cumulative compressive strain history of confined concrete is normalised by its ultimate value (Eq. (24)) to get Normalised Confined Concrete (NCC) index. Therefore, NCC=1 will be corresponding to CC failure. As an example, in Fig. 18 the calculation of NCC for Fig. 17 (c) is illustrated. As can be seen in this figure, the peak compressive strain of confined concrete (ε_{cc}) at each half-cycle of loading history is divided by the corresponding $\varepsilon_{cu,corr}$ (Eq.(24)) to obtain NCC.

The LCF index is the cumulative low-cycle fatigue damage index. To account for this damage index, as explained earlier in the text, the *Fatigue* material available in OpenSees is used. The *Fatigue* material employs the Coffin-Manson fatigue life model (Eq. (12)) to calculate the LCF damage index. The calculated LCF index is a quantity between 0 and 1; where the latter corresponds to LCF failure. In this way, the cumulative damage index of confined concrete will be comparable to that of LCF (because both of them will be in the range of 0 and 1).

As can be seen in Fig. 17, while for the pristine square column neither NCC nor LCF is critical (Fig. 17(a)); all the corroded square columns experience CC failure followed by LCF failure (Figs. 17(b-d)).

This shows that corrosion significantly influences the failure mode of RC columns. Additionally, immediately after the occurrence of the LCF failure, the column cannot withstand further cycles and the area within the afterwards loops become much smaller; i.e. it loses its energy dissipation capability.

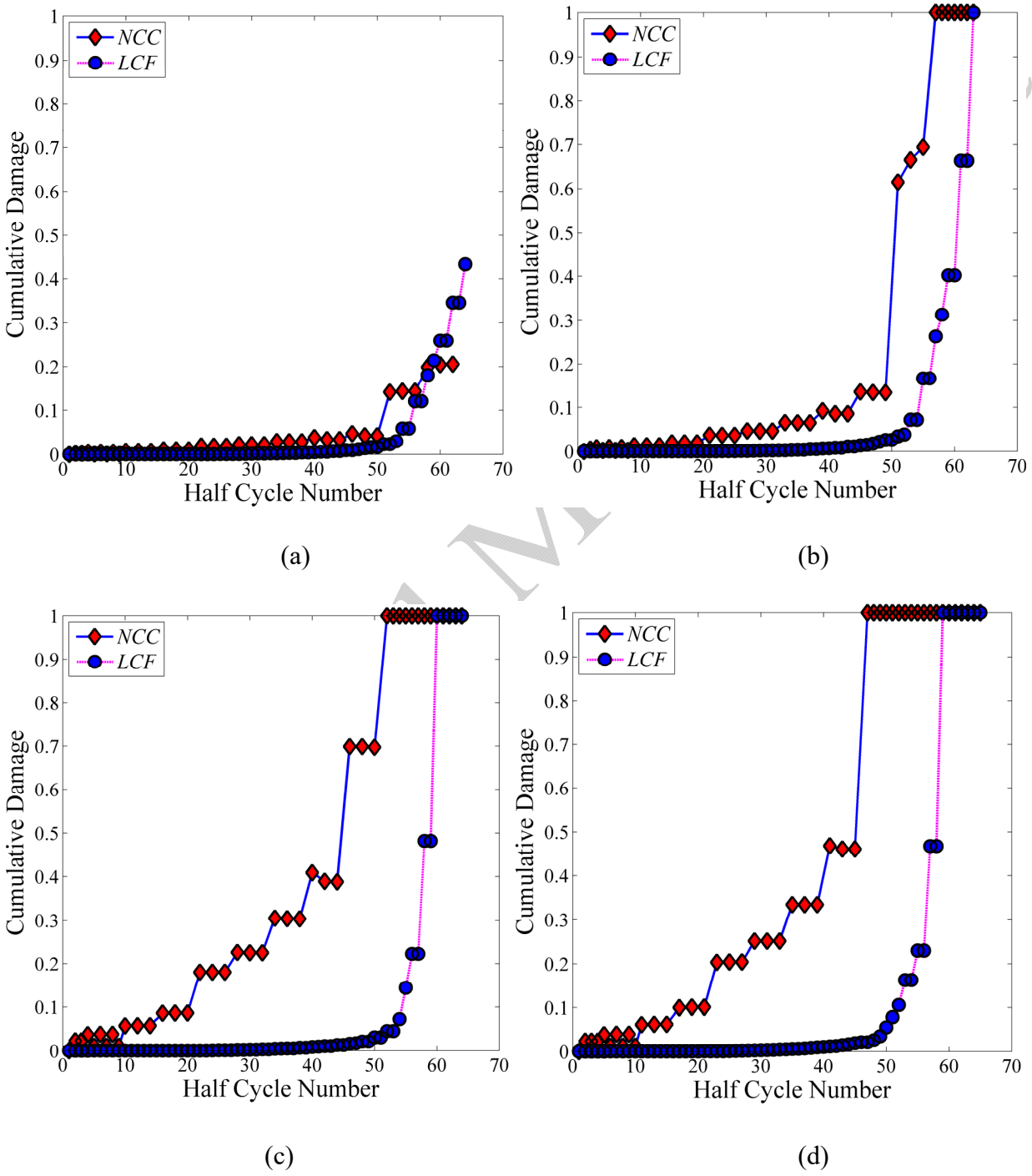

Fig 17. Accumulated damage distribution along with the increased number of cycles: (a) pristine square column; (b) column at t_p=10 years; (c) column at t_p= 30 years, and (d) column at t_p =80 years

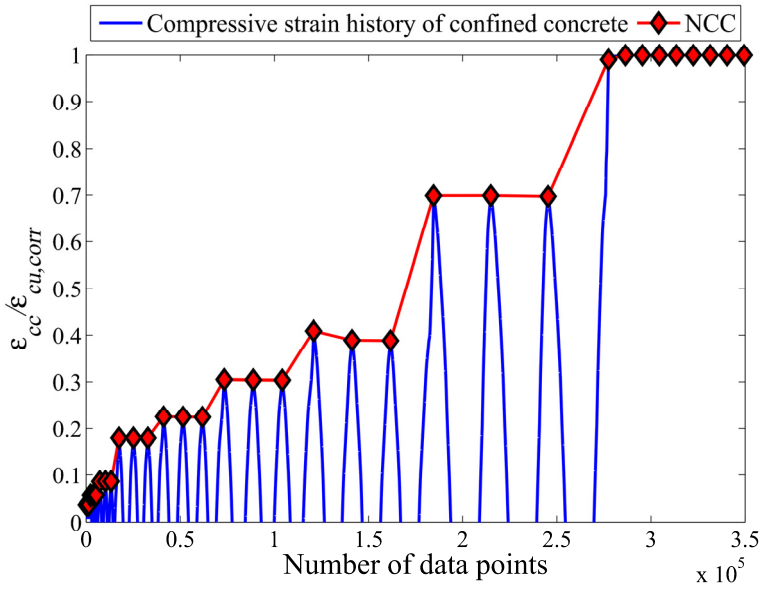

Fig 18. An example of calculating NCC

As discussed earlier in this section, Fig. 16 clearly shows the cyclic degradation of corroded columns comparing to that of the pristine column. This occurs due to the inelastic buckling and LCF degradation of corrosion damaged reinforcing bars that lead to a global pinching response of the corroded columns; and therefore, the energy dissipation capacity of the corrosion damaged columns is significantly degraded.

Fig. 19 compares the cumulative work of considered corrosion damaged square columns with that of pristine square column. In this figure, the cumulative work of each considered column at each half cycle number is normalised to total cumulative work of pristine column to get the normalised cumulative work. As can be seen in Fig. 19, as mass loss percentage increases the energy dissipation capacity of the columns decreases significantly. For example, 22.4 percentage of mass loss (corresponding to t_p= 80 years) results in more than 55% energy dissipation loss.

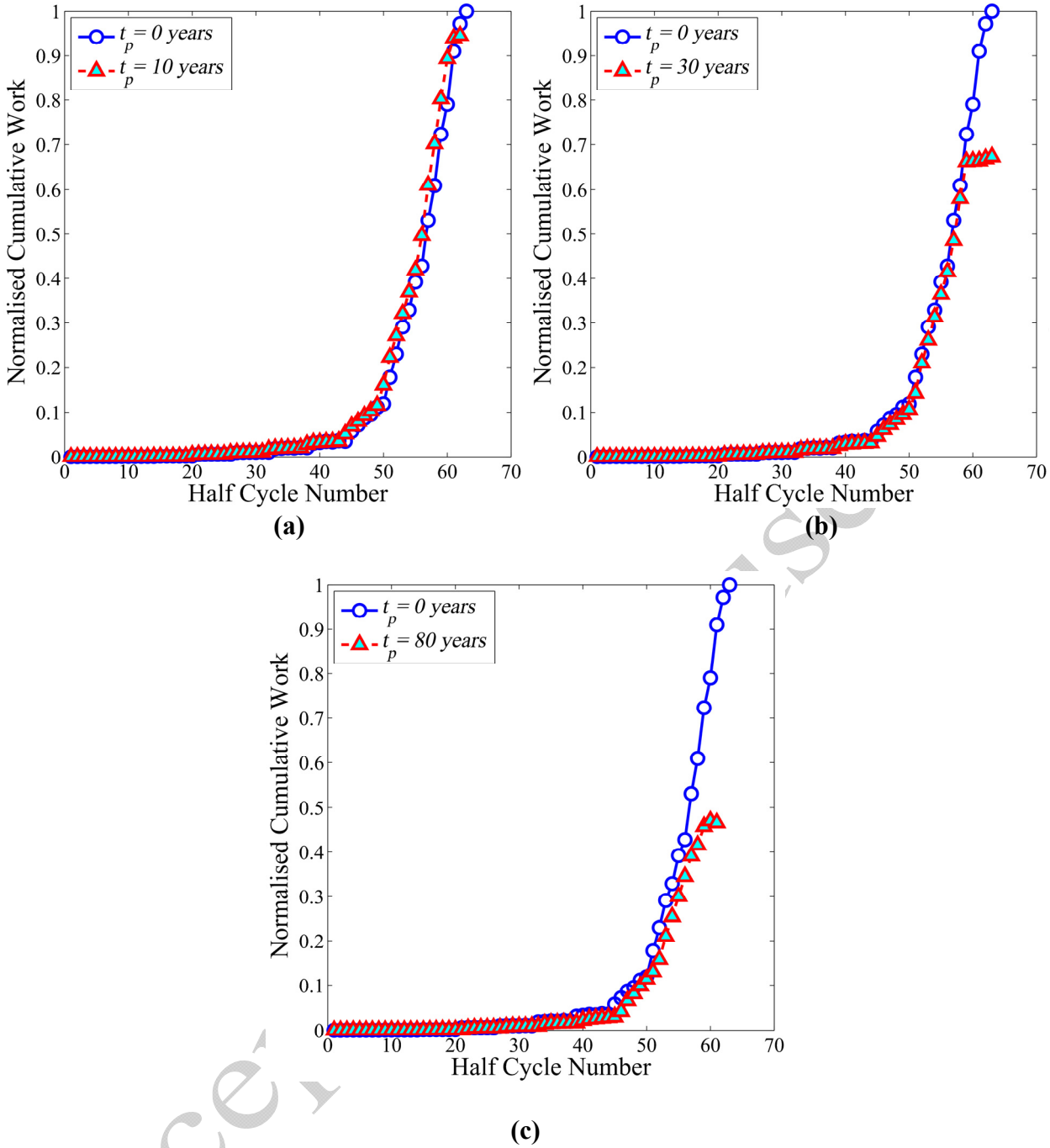

Fig 19. Comparing cumulative energy dissipation of the pristine square column with that of: (a) column at t_p=10 years; (b) column at t_p= 30 years, and (c) column at t_p =80 years

6.2. Proposed circular RC column

Alongside the level of corrosion, however, the geometry of RC structures might influence their failure mode, cyclic behaviour and energy dissipation capacity. To investigate this, another hypothetical RC column with different geometrical details is considered. The details of this hypothetical column are considered to be same as the circular column (Column 415) experimentally tested by Lehman and Moehle (2000). The cross-sectional details of this column, as well as its adopted fibre discretisation, is

shown in Fig. 20. The *Concrete 04* material model (available in OpenSees) is adopted to simulate the nonlinear material response of confined and unconfined concrete. Further details about the geometry and material properties of this column are provided in (Lehman and Moehle 2000).

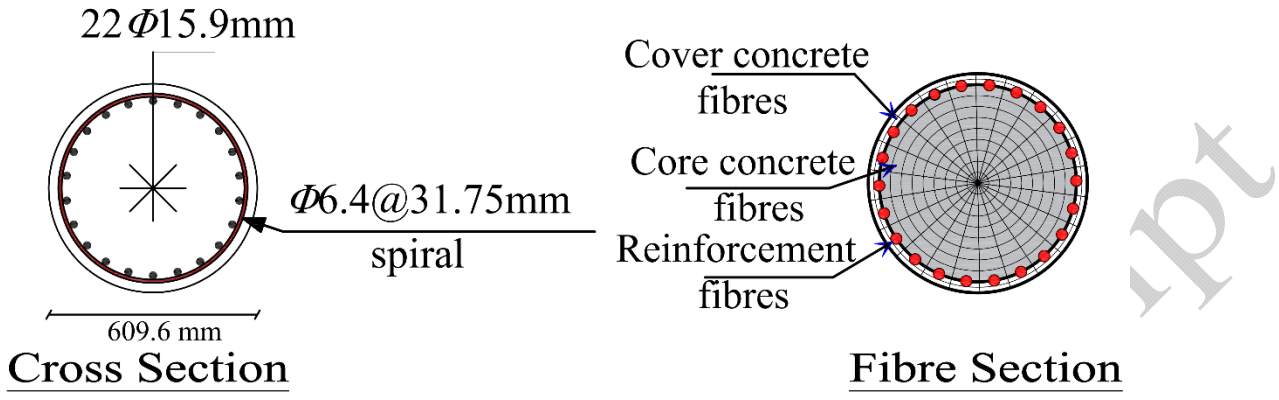

Fig 20. Cross-sectional details and fibre section of hypothetical circular RC column

Using the same percentages of mass losses (Table 3) and loading protocol (Fig. 15), the cyclic analyses are repeated for the hypothetical circular column. The fatigue parameters are kept to be same as those of the square column because the slenderness ratios of both the columns are same (L/D=10).

Figs. (21-22) show the hysteretic loops and damage accumulation of the circular column, respectively. Fig. 21(a) shows that despite the pristine square column, not only the pristine circular column experiences the LCF failure; but also, it happens before CC failure. This most likely because the considered circular column is a well designed (well confined) flexural column; where the confined concrete can sustain higher flexural compressions. On the other hand, the outmost reinforcing bar in the circular section sustains large inelastic strains that result in the accumulation of fatigue damage in it and finally LCF failure.

However, as Figs. 22(b-c) show, with the increasing level of corrosion, the CC failure occurs prior to LCF failure. Even, for severely corroded column (Fig. 22(d)), the CC failure takes place quickly before LCF failure becomes critical. This is because the severe corrosion of spirals reduces the confinement of core concrete significantly; and in practice, the core concrete in the last case (22.4% corrosion) is unconfined.

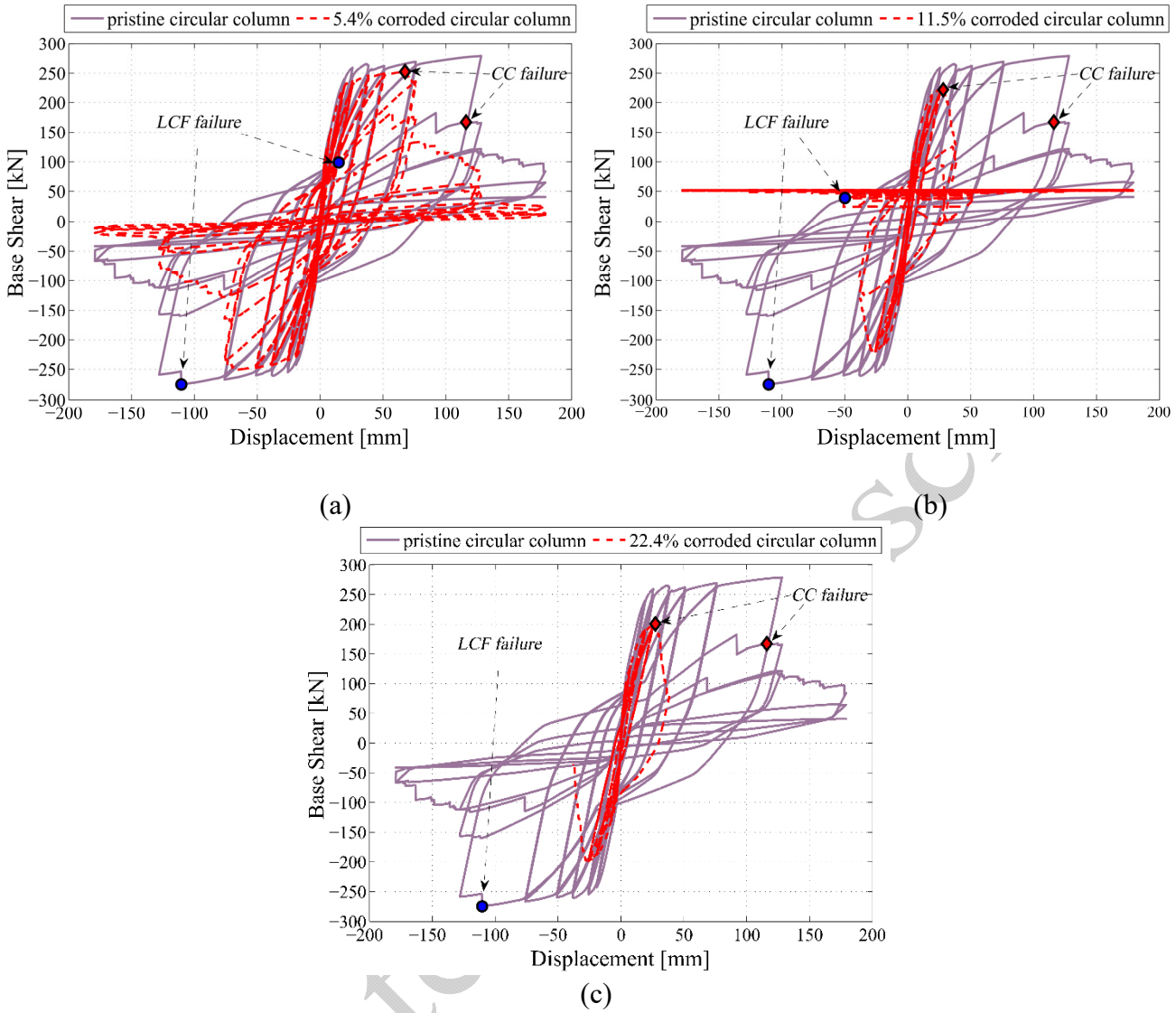

Fig. 21 Comparing hysteretic loops of the pristine circular column with that of: (a) 5.4 % corroded column; (b) 11.5% corroded column, and (c) 22.4% corroded column

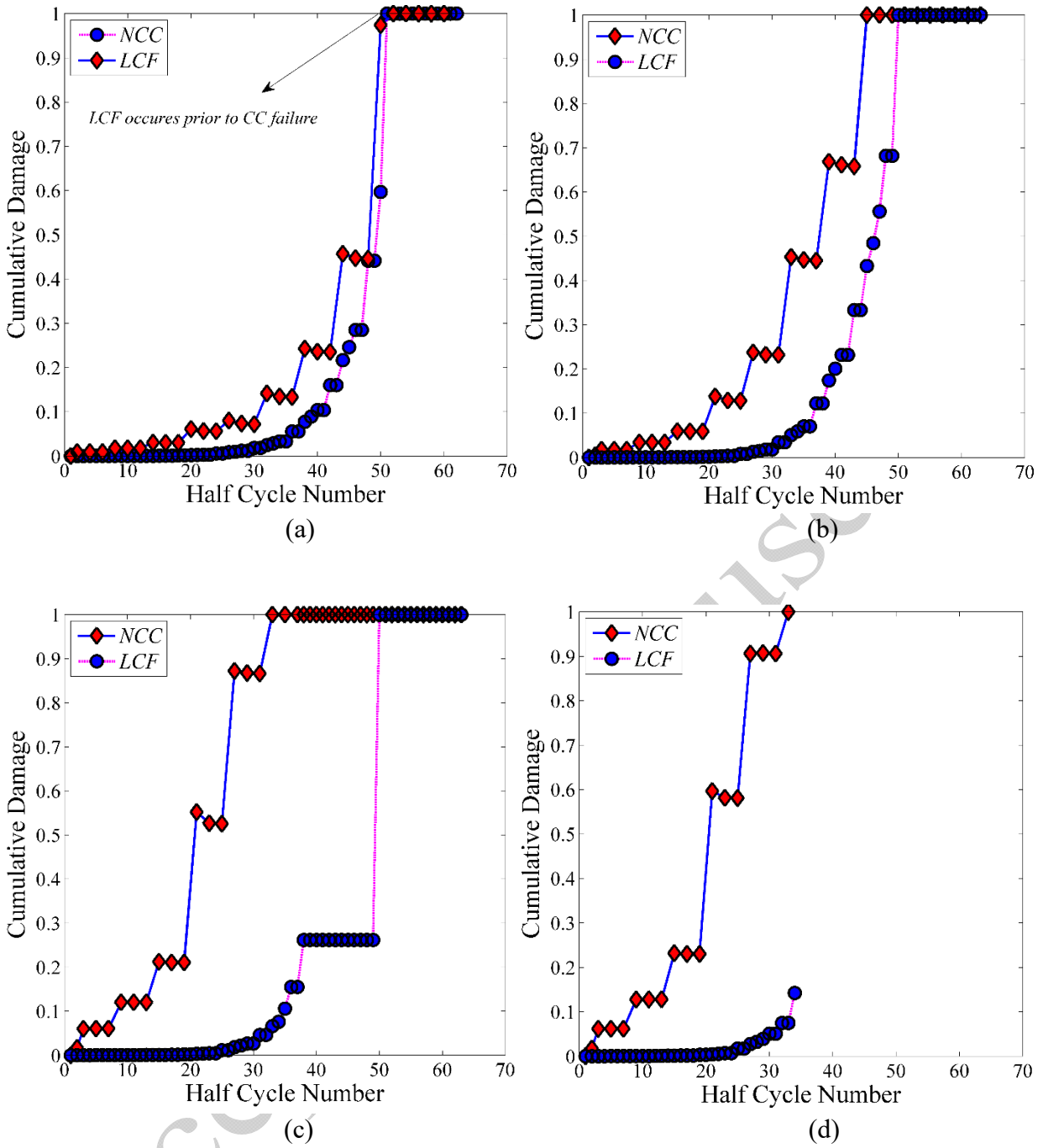

Fig. 22 Accumulated damage distribution along with the increased number of cycles: (a) uncorroded circular column; (b) 5.4 % corroded circular column; (c) 11.5% corroded circular column, and (d) 22.4% corroded circular column

Fig. 23 shows the normalised cumulative work of the hypothetical circular column. This figure shows a significant reduction of energy dissipation capacity of this column; were just 5.4% of corrosion results in more than 30% loss in cumulative energy dissipation (Fig. 23(a)). Moreover, Fig. 23(c) shows a significant reduction in cumulative energy dissipation of severely corroded column by approximately 90% loss.

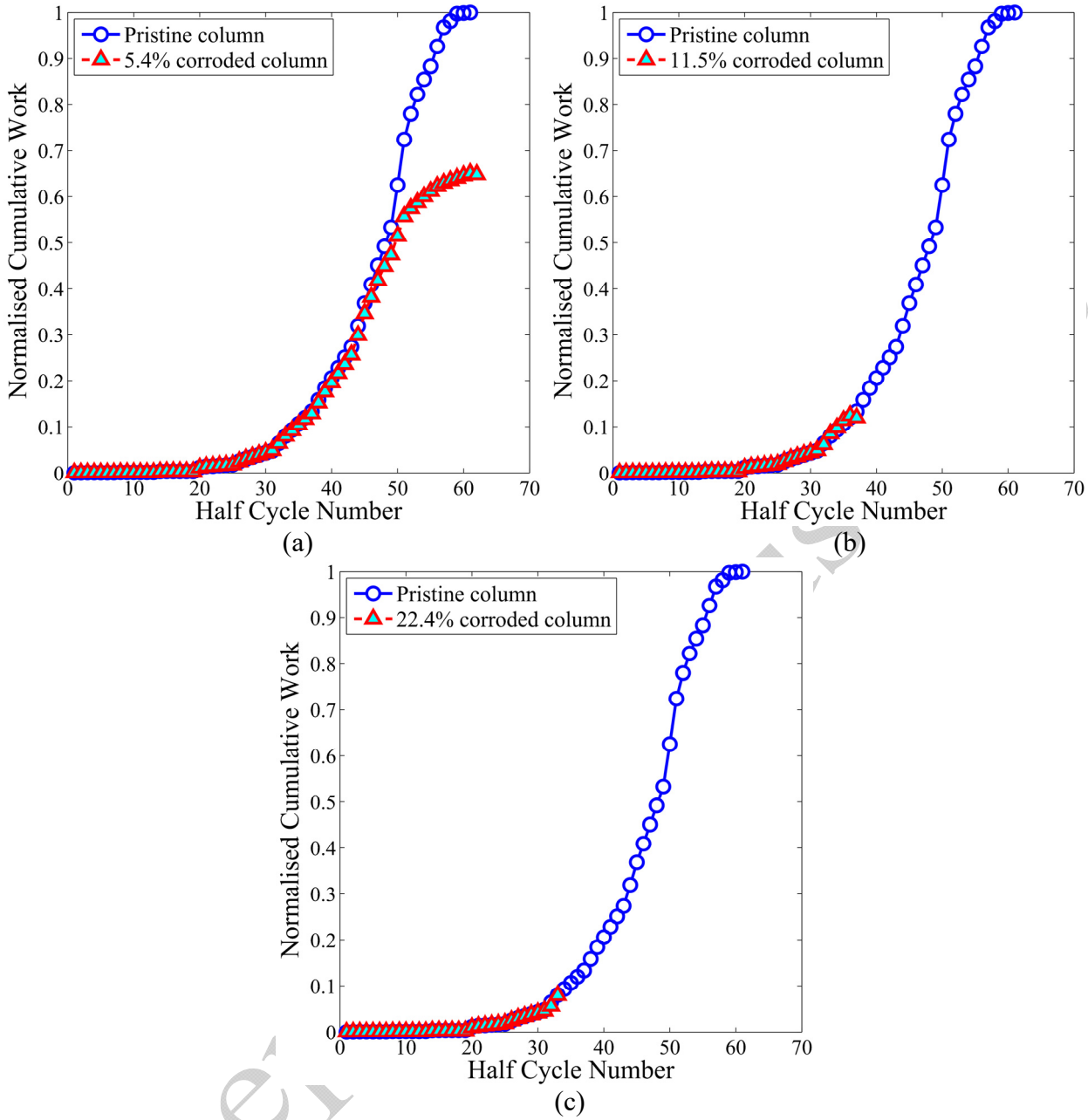

Fig. 23 Comparing cumulative energy dissipation of the pristine circular column with that of: (a) 5.4 % corroded circular column; (b) 11.5% corroded circular column, and (c) 22.4% corroded circular column

7. Nonlinear dynamic response and seismic fragility of corroded RC frames

In this part, a one-bay RC moment-resisting frame is considered as a representative for deteriorated structures that are prone to be subjected to cyclic seismic loading. This frame is designed to meet the requirements of ASCE 7–10 (2010) and ACI 318–14 (2014). The details of the considered RC frame is shown in Fig 24. In this figure, H is the height of cross-section (either column or beam); B is the width of cross-section (either column or beam); ρ_l is the ratio of vertical reinforcement of column; ρ_h is the

ratio of transverse reinforcement; ρ_{top} is the ratio of top longitudinal reinforcement of beam, and ρ_{bot} is the ratio of bottom longitudinal reinforcement of beam. The axial compression load of each column is considered to be 240 kN.

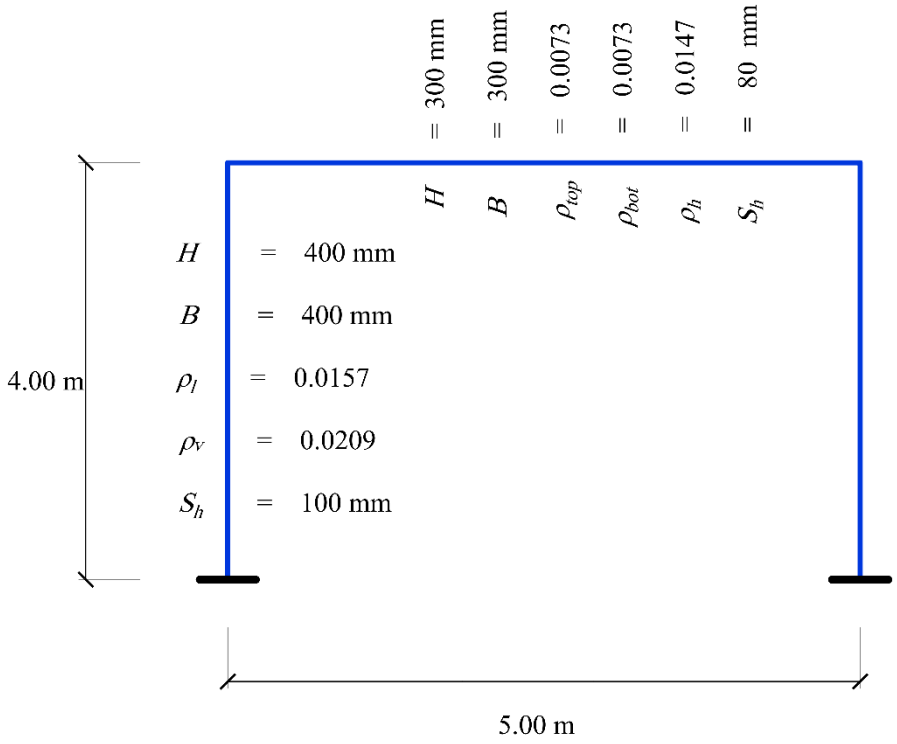

Fig 24. Geometry and details of hypothetical RC frame

The structural behaviour of the hypothetical RC frame is simulated using the NFEMT shown in Fig 11. The details of material properties are tabulated in Table 4. To investigate the impact of corrosion on the nonlinear dynamic response of the considered RC frame, in addition to a pristine frame (ψ=0), a 15% corroded frame is also considered (ψ=15%).

Table 4. Material properties of the hypothetical RC frame

Material Properties	$\sigma_{y,0}$ [MPa]	$\sigma_{yt,0}$ [MPa]	$\sigma_{u,0}$ [MPa]	$\varepsilon_{u,0}$	E_s [MPa]	σ_c [MPa]
	400	340	600	0.18	210000	30

Fig. 25 compares the pushover analysis results of the considered corroded frame with that of the pristine frame. In this figure, the normalised base shear is the ratio of base shear of each column to the maximum base shear of the uncorroded frame. Fig. 25 shows that the flexural capacity of corroded frame is 20%

less than that of the pristine frame. Same to Fig. 13, Fig. 25 confirms that corrosion adversely affects the DS. Therefore, in the absence of clear guidelines for DS of corrosion damaged structures, the associated drift of CC failure is adopted here as complete collapse damage DS to plot the fragility curve of the corroded frame. Moreover, for the pristine frame, 8% of drift is considered as the collapse DS as per the recommendation of HAZUS- MH MR5 (2010) for RC frames.

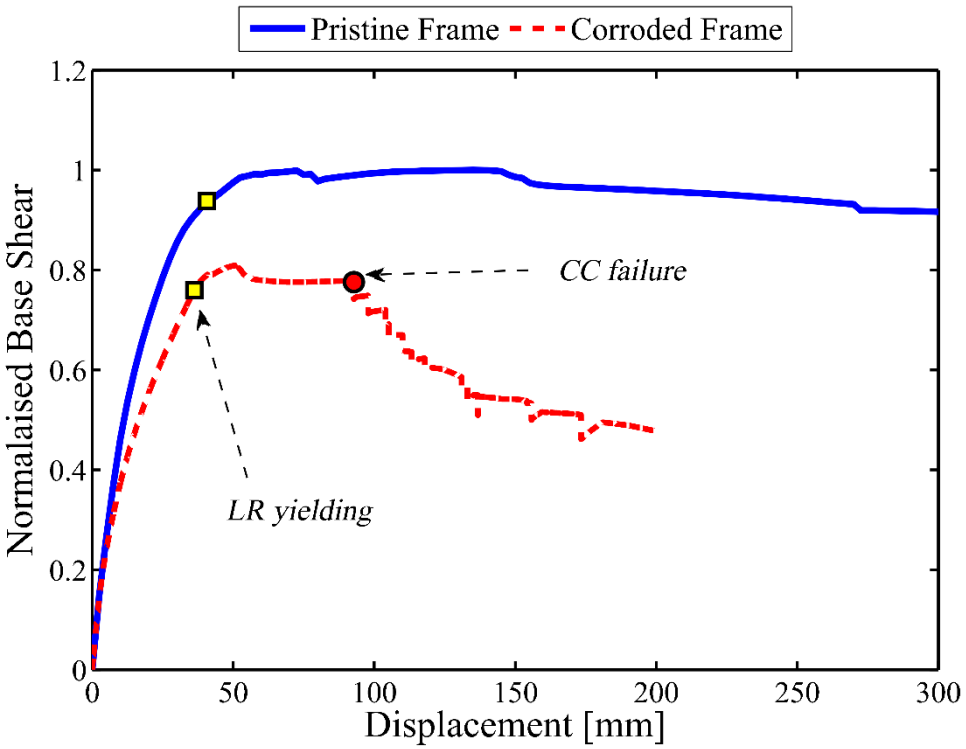

Fig 25. Results of pushover analyses of the hypothetical RC frame

To study the nonlinear dynamic response of the considered pristine and corroded frames, IDA is implemented. In this regard, a suite of 10 ground motion records is taken from FEMA P695 (2009). The list of selected earthquake records is presented in Table 5. Each ground motion record is applied to the RC frame by a series of increasing scale factors. Spectral acceleration at the fundamental period of the structure (Sa(T_1)) is adopted as Intensity Measure (IM), and maximum drift percentage of roof (θ_{max}) is considered as Damage Measure (DM). The acceleration spectrum of the selected record suite is shown in Fig. 26.

Table 5. Selected Ground motion records

No.	Event	Year	Station Name	Magnitude (M_w)	PGA (g)
1	Kobe, Japan	1995	Nishi-Akashi	6.9	0.51
2	Kobe, Japan	1995	Shin-Osaka	6.9	0.24
3	Kocaeili, Turkey	1999	Duzce	7.5	0.36
4	Kocaeli, Turkey	1999	Arcelik	7.5	0.22
5	Landers	1992	Yermo Fire Station	7.3	0.24
6	Landers	1992	Coolwater	7.3	0.42
7	Loma Prieta	1989	Capitola	6.9	0.53
8	Loma Prieta	1989	Gilroy Array #3	6.9	0.56
9	Manjil, Iran	1990	Abbar	7.4	0.51
10	Superstition Hills	1987	El Centro Imp. Co.	6.5	0.36

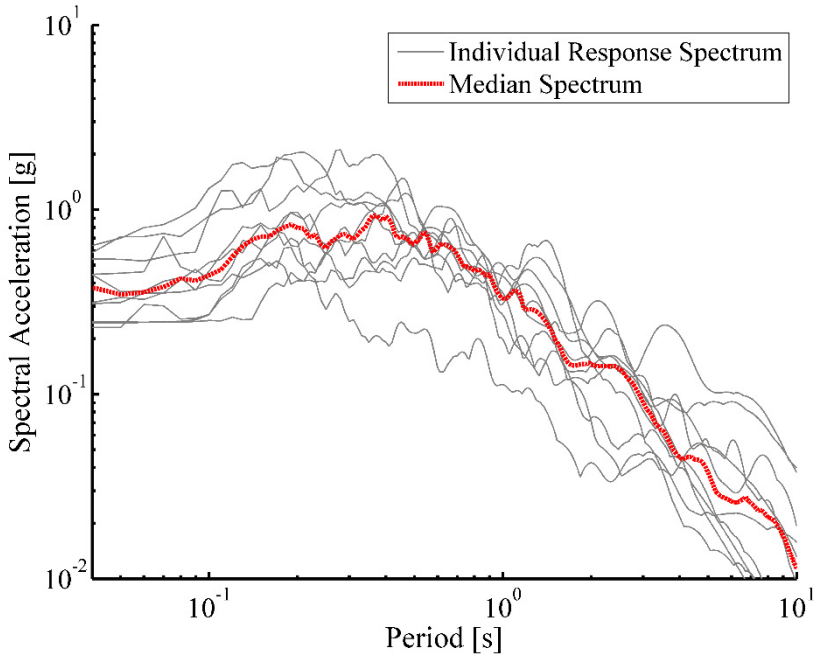

Fig 26. Acceleration spectrum of the selected ground motion suite

Fig. 27 shows the results of IDA for each record and summarised result (Median curve). In Fig. 27(c), the medina IDA curves of hypothetical pristine and corroded frames are compared. As Fig. 27(c) shows the spectral acceleration response of corroded frame is significantly reduced in comparison with that of a pristine frame. This is because, as discussed in section 5, due to the premature inelastic bucking and LCF failure of corroded reinforcing bars, the energy dissipation capacity of corroded structures is considerably lower than the virgin structures. Therefore, the corroded structure is highly degraded at lower IMs and cannot sustain higher intensities of earthquakes.

In HAZUS-MH MR5 (2010) the damage limit states for low-rise RC frames are presented in terms of θ_{max}, where θ_{max}= 0.01 corresponds to slight damage limit state, θ_{max}= 0.03 corresponds to moderate damage limit state, θ_{max}= 0.05 corresponds to extensive damage limit state, and θ_{max}= 0.08 corresponds to complete collapse damage limit state. For each damage limit state, a detailed definition is provided in HAZUS-MH MR5 (2010). For example, the complete collapse damage limit state is associated with the crushing of confined concrete or fracture of longitudinal reinforcement, whichever takes place first. Here to compare the failure probability (probability of exceeding complete collapse DS) of the considered pristine and corroded frame, using the output of IDAs and mass loss-dependent complete collapse DS (from Fig. 25), the fragility curves are plotted employing the fragility function presented in Eq. (27):

$$P\left[\theta_{max} \geq DS_i \mid Sa(T_1) = y\right] = 1 - \Phi\left(\frac{\ln(DS_i) - \mu_{ln}}{\sigma_{ln}}\right) \tag{27}$$

Where the left side of the equation represents the probability that θ_{max} exceeds i^{th} DS (DS_i) given that $Sa(T_1)=y$. In Eq. (27), it has been assumed that the values of θ_{max} corresponding to $Sa(T_1)=y$ follow a lognormal distribution (Φ) with logarithmic mean of μ_{ln} and logarithmic standard deviation of σ_{ln}. Here, for the corroded frame, the complete collapse DS is considered to be 0.023 which is the corresponding drift ratio of CC failure according to the results presented in Fig. 25. For the uncorroded frame, the complete collapse DS is considered to be 0.08 (HAZUS-MH MR5 (2010)).

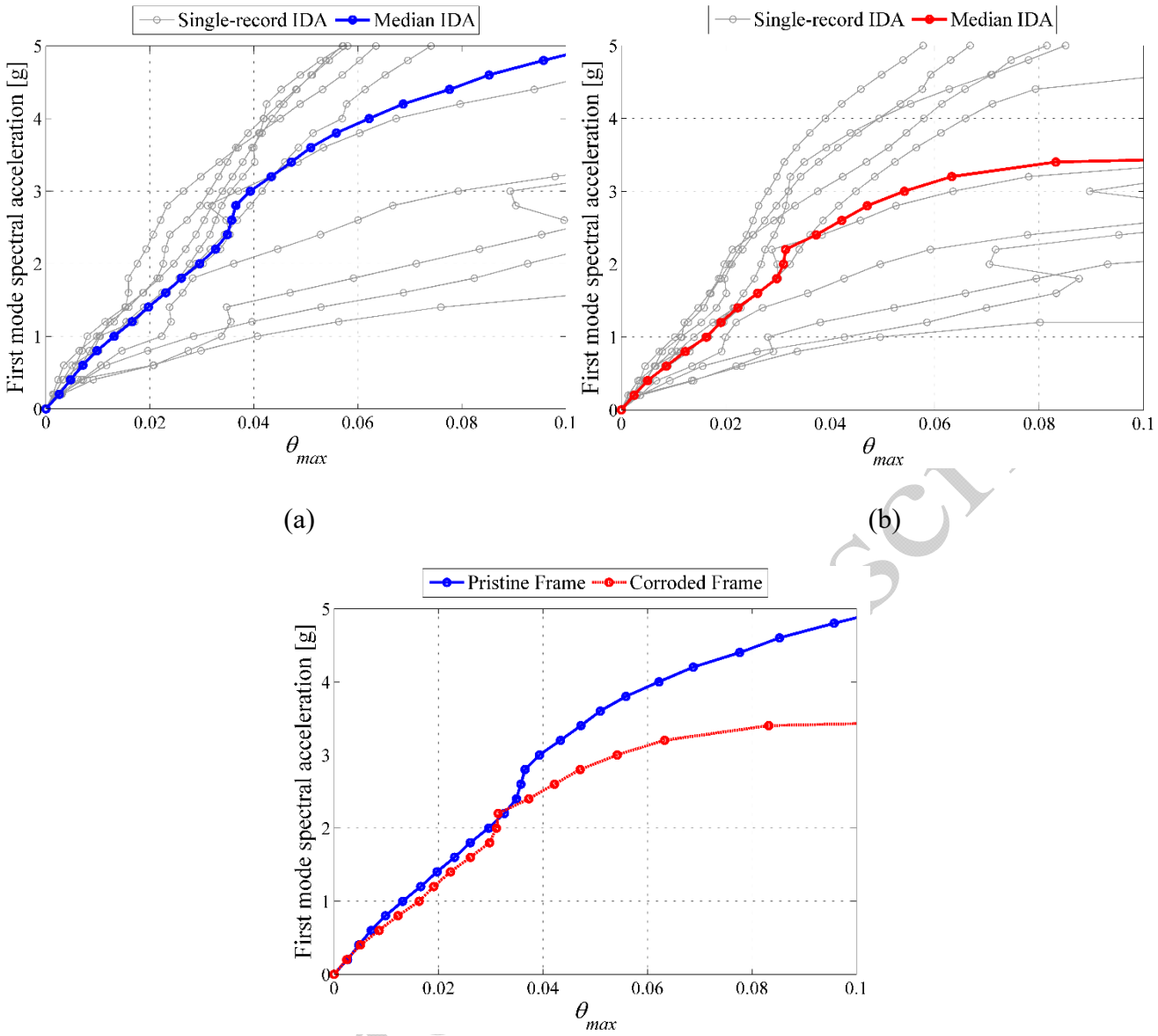

Fig 27. Results of IDA: (a) Pristine frame; (b) corroded frame; (c) Median IDAs

Fig. 28 shows the fragility curves for both the frames. To emphasis on the importance of considering the DS of corroded structures as a corrosion-dependent parameter, in this figure the fragility curve of the corroded frame is plotted based on two different DSs: firstly based on the corrosion-dependent DS (i.e. 0.023 for the corroded frame in Fig. 28(a)), and then using the traditional approach that is based on the DS of the pristine frame (i.e. 0.08 for both the frames in Fig. 28(b)). As can be seen in Fig. 28, the probability of failure for a given intensity of an earthquake is significantly higher for the corroded frame. Moreover, comparing Fig. 28(a) with Fig. 28(b), it can be seen that the traditional approach (which is

based on the corrosion-independent damage limit states proposed in HAZUS-MH MR5 (2010)) significantly underestimates the failure probability of the corroded frame. For instance, while based on the corrosion-dependent DS the probability of failure of the corroded frame for Sa(T_1)=3g is more than 95%; it is approximately 55% based on the traditional DS.

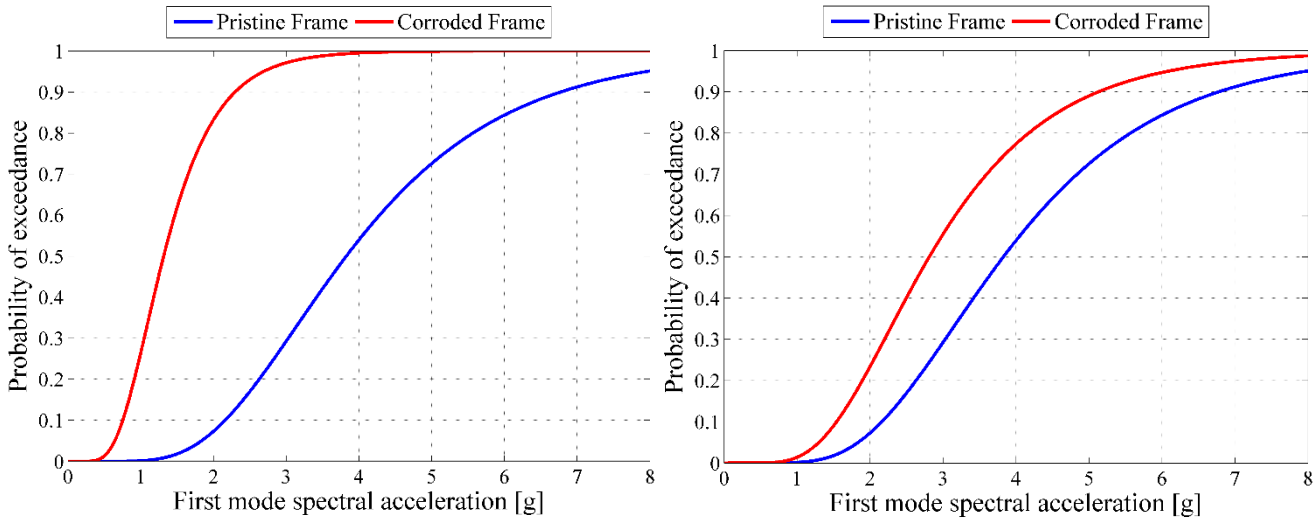

(a) (b)

Fig. 28 Fragility curves of considered RC frames: (a) corrosion-dependent DS; (b) corrosion-independent DS

8. Conclusion

In this paper, a modelling guideline for structural analysis and fragility assessment of deteriorated RC structures is presented. Firstly, empirical and analytical equations are introduced to consider the adverse influence of corrosion on material behaviour. Then, the proposed NFEMT for nonlinear static and dynamic analysis of RC columns and RC frames is presented. Finally, using the proposed model, nonlinear static (pushover and cyclic) and IDAs are conducted on two hypothetical RC columns and a hypothetical RC frame. The outcome of the current study shows that the proposed modelling guidelines will enable the engineering community to predict the complex nonlinear behaviour and capture multiple failure modes of deteriorated RC structures. The main findings of this paper can be summarised as follows:

- Corrosion of reinforcement changes the failure mode of RC structures. LCF failure of reinforcement is much more critical in corroded RC structures subject to earthquake loading.
- Energy dissipation capacity, ductility and flexural capacity of corroded RC structures are significantly reduced compared to those of pristine structures.
- While for the pristine square column neither NCC nor LCF is critical, all the corroded square columns experience CC failure followed by LCF failure.
- While in the pristine circular column the CC failure is preceded by LCF failure, in severely corroded circular RC column the CC failure is much more critical than LCF failure due to the premature fracture of confining steel.
- Corroded structures can fail at a low amplitude of seismic loading due to the significant reduction of their strength and ductility.
- The probability of failure of corroded RC structures is much higher than that of pristine structure for a given IM. For example, 15 % of corrosion results in approximately 60 % increase in the probability of failure under Sa(T_1)=4g.

References

ACI Committee 318. 2014. Building Code Requirements for Structural Concrete (ACI 318- 14) and Commentary on Building Code Requirements for Structural Concrete (ACI 318R-14). Farmington Hills, MI: American Concrete Institute.

Afsar Dizaj, E., Kashani, M.M. 2020. Numerical investigation of the influence of cross-sectional shape and corrosion damage on failure mechanisms of RC bridge piers under earthquake loading. Bulletin of Earthquake Engineering, 18, 4939–4961. https://doi.org/10.1007/s10518-020-00883-3.

American Society of Civil Engineers (ASCE). 2010. Minimum design loads for buildings and other structures, ASCE 7-10, Reston, VA.

Alipour, A., Shafei, B., Shinozuka, M. 2011. "Performance evaluation of deteriorating highway bridges located in high seismic areas." Journal of Bridge Engineering. 6: 597-611.

Anam, I., and Shoma, ZN. 2002. “Nonlinear Properties of Reinforced Concrete Structures.” Dhaka, The University of Asia Pacific.

Apostolopoulos, C.A., Papadopoulos, M.P., Pantelakis, S.G. 2006. “Tensile behavior of corroded reinforcing steel bars BSt 500s.” Construct and Build Mater. 20(9): 782–789.

Apostolopoulos, C.A. 2007. “Mechanical behavior of corroded reinforcing steel bars S500s tempcore under low cycle fatigue.” Construct and Build Mater. 21: 1447–1456.

Aquino, W., Hawkins, NM. 2007. “Seismic Retrofitting of Corroded Reinforced Concrete Columns Using Carbon Composites.” ACI Structural Journal. 104(3): 348-356.

Balan, T.A., Filippou, F.C., and Popov, E.P. 1998. “Hysteretic model of ordinary and high-strength reinforcing steel.” Journal of Structural Engineering. 124(3): 288–297.

Belletti, B., Stocchi, A., Scolari, M., Vecchi, F. 2017. “Validation of the PARC_CL 2.0 crack model for the assessment of the nonlinear behaviour of RC structures subjected to seismic action: SMART 2013 shaking table test simulation”. Engineering Structures, 150: 759–773.

Belletti, B., Vecchi, F. 2018. “Implementation of Steel Constitutive Model Including Buckling in ARC_CL 2.1 Crack Model”. 5th International fb Congress. Melbourne, Australia.

Berry MP, Eberhard MO. Performance modelling strategies for modern reinforced concrete bridge columns. PEER research report. Univ. of Calif. Berkeley; 2006. 67(11).

Cairns, J., Plizzari, GA., Du, YG., Law, DW., Chiara, F. 2005. “Mechanical properties of corrosion-damaged reinforcement.” ACI Mat J. 102 (4): 256–264.

California Department of Transportation (Caltrans). 2010. Seismic Design Criteria (SDC), version 1.6, Sacramento, CA.

Coleman, J., Spacone, E. 2001. “Localisation issues in force-based frame elements.” J Struct Eng 2001;127(11):1257–65.

Coronelli, D., Gambarova, P. 2004. “Structural assessment of corroded reinforced concrete beams: modelling guidelines.” J Struct Eng. 130 (8): 1214-1224.

Darmawna, MS. 2010. “Pitting corrosion model for reinforced concrete structures in a chloride environment.” Mag. Concr. Res. 62 (2): 91–101.

Dhakal, R., and Maekawa, K. 2002. “Modeling for postyield buckling of reinforcement.” Journal of Structural Engineering.” 128(9): 1139–1147.

Di Carlo, F., Meda, A., Rinaldi, Z. 2017. “Numerical evaluation of the corrosion infuence on the cyclic behaviour of RC columns.” Eng Struct. 53:264–278.

Dizaj, E.A., Madandoust, R., Kashani, M.M. 2018a. “Exploring the impact of chloride-induced corrosion on seismic damage limit states and residual capacity of reinforced concrete structures.” Struct Infrastruct Eng. 14(6): 714–29.

Dizaj, E.A., Madandoust, R., Kashani, MM. 2018b. “Probabilistic seismic vulnerability analysis of corroded reinforced concrete frames including spatial variability of pitting corrosion.” Soil Dynamics and Earthquake Engineering. 114: 97–112.

Du, YG., Clark, L.A., Chan, AHC. 2005a. “Residual capacity of corroded reinforcing bars.” Magazine of Conc Res. 57 (3):135–147.

Du, Y.G., Clark, L.A., Chan, AHC. 2005b. “Effect of corrosion on ductility of reinforcing bars.” Magazine of Conc Res. 57 (7): 407–419.

FEMA P695: Quantification of Building Seismic Performance Factors. 2009. Federal Emergency Management Agency, Washington, DC.

Fernandez, I., Bairan, J.M., and Mari, A.R. 2015. “Corrosion effects on the mechanical properties of reinforcing steel bars. Fatigue and σ-ε behaviour.” Construction and Building Materials. 101, 772–783.

Ge, X., Dietz, M.S., Alexander, N.A. *et al.* 2020. Nonlinear dynamic behaviour of severely corroded reinforced concrete columns: shaking table study. Bulletin of Earthquake Engineering, 18, 1417–1443. https://doi.org/10.1007/s10518-019-00749-3.

Ghosh, J., and Padgett. JE. 2010. “Aging considerations in the development of time-dependent seismic fragility curves.” Journal of Structural Engineering. 136(12): 1497-1511.

Guo, A., Yuan, W., Lan, Ch., Guan, X., Li, H. 2015a. “Experimental investigation on the cyclic performance of reinforced concrete piers with chloride-induced corrosion in marine environment.” Engineering Structures. 105: 1-11.

Guo, A., Yuan, W., Lan, Ch., Guan, X., Li, H. 2015b. “Time-dependent seismic demand and fragility of deteriorating bridges for their residual service life.” Bulletin of Earthquake Engineering. 13(8): 2389-2409.

HAZUS-MH MR5. 2010. Earthquake loss estimation methodology. Technical and User’s Manual. Department of Homeland Security, Federal Emergency Management Agency, Mitigation Division. Washington D.C.

Jeon, J. S., Lowes, L. N., DesRoches, R., & Brilakis, I. (2015). Fragility curves for non-ductile reinforced concrete frames that exhibit different component response mechanisms. *Engineering Structures, 85*, 127–143.

Kashani, M.M., Barmi, AK., Malinova, S. 2015b. “Influence of inelastic buckling on low-cycle fatigue degradation of reinforcing bars.” Construction and Building Materials. 94: 644-655.

Kashani, M.M., Crewe, A.J., and Alexander, N.A. 2013a. “Nonlinear cyclic response of corrosion-damaged reinforcing bars with the effect of buckling.” Construction and Building Materials. 41:388–400.

Kashani, M.M., Crewe, A.J., and Alexander, N.A. 2013b. “Use of a 3D optical measurement technique for stochastic corrosion pattern analysis of reinforcing bars subjected to accelerated corrosion.” Corrosion Science. 73: 208–221.

Kashani, M.M., Lowes, L.N., Crewe, A.J., Alexander, N.A. 2015a. “Phenomenological hysteretic model for corroded reinforcing bars including inelastic buckling and low-cycle fatigue degradation.” Comput Struct. 156: 58-71.

Kashani, M.M., Lowes, L.N., Crewe, A.J., Alexander, N.A. 2016. “Nonlinear fibre element modelling of RC bridge piers considering inelastic buckling of reinforcement.” Eng Struct.116: 163-177.

Kashani, M.M., Maddocks, J., Afsar Dizaj, E. 2019. “Residual Capacity of Corroded Reinforced Concrete Bridge Components: A State-of-the-Art Review.” Journal of Bridge Engineering. 24(7): 03119001.

Lehman, DE., Moehle, JP. 2000. “Seismic performance of well-confined concrete columns.” PEER research report. Univ. of Calif. Berkeley.

Mander, JB., Priestley, MJN., Park, R. 1988. “Theoretical stress-strain model for confined concrete.” J Struct Eng. 114 (8): 1804-1825.

Manson SS. 1965. “Fatigue: A complex subject-Some simple approximations.” Exp Mech. 5 (7): 193–226.

Ma, Y., Che, Y., and Gong, J. 2012. “Behaviour of corrosion damaged circular reinforced concrete columns under cyclic loading.” Construction and Building Materials. 29: 548-556.

McKenna, F. 2011. “OpenSees: a framework for earthquake engineering simulation.” Computing in Science & Engineering. 13(4): 58-66.

Meda, A., Mostosi, S., Rinaldi, Z., Riva, P. 2014. “Experimental evaluation of the corrosion influence on the cyclic behaviour of RC columns.” Engineering Structures. 76: 112-123.

Park, R., Paulay, T. 1990. “Use of Interlocking Spirals for Transverse Reinforcement in Bridge Columns, Strength and Ductility of Concrete Substructures of Bridges.” RRU (Road Research Unit) Bulletin 84.

Priestley, M., Paulay, T. 1992. “Seismic design of reinforced concrete and masonry buildings. New York: John Wiley & Sons, Inc.

Pugh, JS. Numerical simulation of walls and seismic design recommendations for walled buildings [Ph.D. thesis]. University of Washington; 2012.

Rao, A.S., Lepech, M.D., Kiremidjian, A.S., and Sun, X.-Y.2016. “Simplified structural deterioration model for reinforced concrete bridge piers under cyclic loading.” Structure and Infrastructure Engineering. 13(1): 55–66.

Rodriguez, J., Ortega, LM., and Casal, J. 1997. “Load carrying capacity of concrete structures with corroded reinforcement.” Construction and Building Materials. 11(4): 239-248.

Scott, B.D., Park, R., Priestley, MJN. 1982. “Stress-strain behavior of concrete confined by overlapping hoops at low and high strain rates.” ACI J. 79 (1): 13-27.

Spacone, E., Filippou, F.C., and Taucer, F.F. 1996. “Fibre beam-column model for non-linear analysis of R/C frames: part I. formulation.” Earthquake Engineering & Structural Dynamics. 25(7):711-725.

Stewart, MG., Suo, Q. 2009. “Extent of spatially variable corrosion damage as an indicator of strength and time-dependent reliability of RC beams.” Eng. Struct. 31: 198–207.

Steward, MG. 2009. “Mechanical behaviour of pitting corrosion of flexural and shear reinforcement and its effect on structural reliability of corroding RC beams.” Struct.Saf. 31: 19–30.

Tanaka, H., Park, R. 1990. “Effect of Lateral Confining Reinforcement on the Ductile Behavior of Reinforced Concrete Column.” Department of Civil Engineering, University of Canterbury.

Vidal, T., Castel, A., Francois, R. 2004. “Analysing crack width to predict corrosion in reinforced concrete.” Cement Concrete Res. 34(1): 165-174.

Vu, NS., Yu, B., and Li, B. 2017. “Stress-strain model for confined concrete with corroded transverse reinforcement.” Engineering Structures. 151: 472–487.

Xu, J., Wu, G., Feng, D., Cotsovos, D.M., Lu, Y. 2020. “Seismic fragility analysis of shear-critical concrete columns considering corrosion induced deterioration effects.” Soil Dynamics and Earthquake Engineering. 134: https://doi.org/10.1016/j.soildyn.2020.106165.

Yao, L., Shi-ping, Y., Wen-jie, C. 2019. “Seismic behavior of corrosion-damaged RC columns strengthened with TRC under a chloride environment.” Construction and Building Material. 201: 736-745.

Zhao, J., Sritharan, S. 2007. “Modeling of strain penetration effects in fiber-based analysis of reinforced concrete structures.” ACI Structural Journal. 104(2):133–41.

Zhou, H., Xu, Y., Peng, Y., Liang, X., Li, D., Xing, F. 2020. “Partially corroded reinforced concrete piers under axial compression and cyclic loading: An experimental study.” Engineering Structures, 203: https://doi.org/10.1016/j.engstruct.2019.109880.